Short Article

Cell Metabolism

2-Hydroxyglutarate Inhibits ATP Synthase and mTOR Signaling

Graphical Abstract

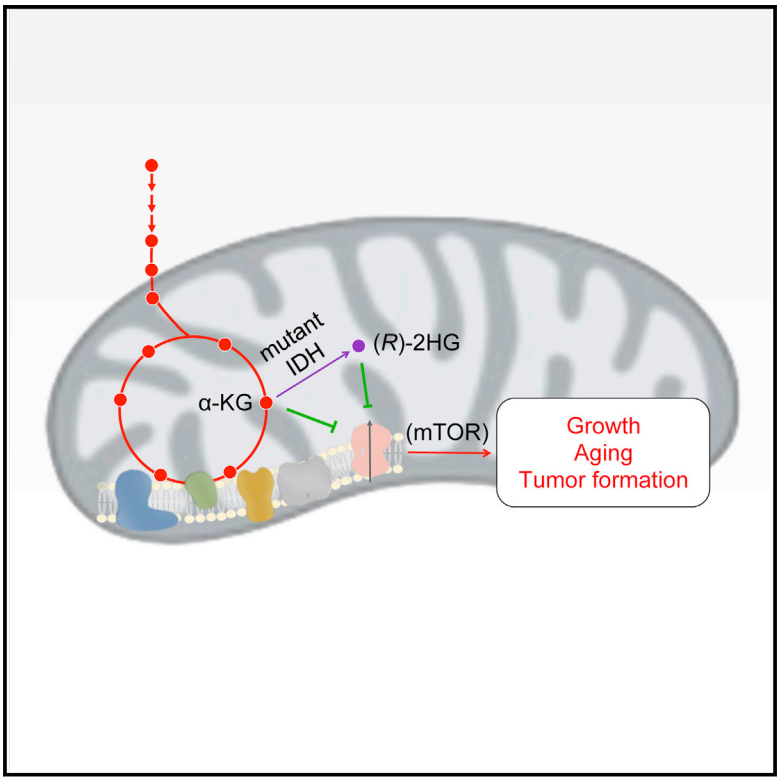

Authors

Xudong Fu, Randall M. Chin, Laurent Vergnes, ..., Michael E. Jung, Karen Reue, Jing Huang

Correspondence

jinghuang.ucla@gmail.com

In Brief

Aberrant isocitrate dehydrogenase enzymes encoded by cancer-associated IDH1 and IDH2 gene mutations produce an oncometabolite, (*R*)-2HG. Fu et al. discover a growth-suppressive function of (*R*)-2-HG mediated by its binding and inhibition of ATP synthase. The resulting OXPHOS perturbation imparts extra vulnerability to glucose limitation in IDH mutant glioblastoma cells.

Highlights

- 2-HG, like α-KG, inhibits ATP synthase and extends the lifespan of *C. elegans*
- IDH1(R132H) mutant cells have reduced ATP content, respiration, and mTOR signaling
- IDH1(R132H) mutant cells exhibit an intrinsic vulnerability to glucose limitation
- ATP synthase is a target of 2-HG's growth-suppressive activity in IDH mutant cells

Fu et al., 2015, Cell Metabolism *22*, 508–515
September 1, 2015
http://dx.doi.org/10.1016/j.cmet.2015.06.009

CellPress

CellPress

Cell Metabolism
Short Article

2-Hydroxyglutarate Inhibits ATP Synthase and mTOR Signaling

Xudong Fu,[1] Randall M. Chin,[2] Laurent Vergnes,[3] Heejun Hwang,[1] Gang Deng,[4] Yanpeng Xing,[4] Melody Y. Pai,[2] Sichen Li,[5] Lisa Ta,[1] Farbod Fazlollahi,[6] Chuo Chen,[7] Robert M. Prins,[8] Michael A. Teitell,[2,9,10] David A. Nathanson,[1] Albert Lai,[5] Kym F. Faull,[6] Meisheng Jiang,[1] Steven G. Clarke,[2,4] Timothy F. Cloughesy,[5,10] Thomas G. Graeber,[1,10,11,12] Daniel Braas,[1,11] Heather R. Christofk,[1,10,11] Michael E. Jung,[1,2,4,10] Karen Reue,[2,3] and Jing Huang[1,2,10,*]

[1]Department of Molecular and Medical Pharmacology, David Geffen School of Medicine, University of California Los Angeles, Los Angeles, CA 90095, USA
[2]Molecular Biology Institute, University of California Los Angeles, Los Angeles, CA 90095, USA
[3]Department of Human Genetics, David Geffen School of Medicine, University of California Los Angeles, Los Angeles, CA 90095, USA
[4]Department of Chemistry and Biochemistry, University of California Los Angeles, Los Angeles, CA 90095, USA
[5]Department of Neurology, David Geffen School of Medicine, University of California Los Angeles, Los Angeles, CA 90095, USA
[6]Pasarow Mass Spectrometry Laboratory, Department of Psychiatry and Biobehavioral Sciences, and Semel Institute for Neuroscience and Human Behavior, University of California Los Angeles, Los Angeles, CA 90095, USA
[7]Department of Biochemistry, University of Texas Southwestern Medical Center, Dallas, TX 75390, USA
[8]Department of Neurosurgery, David Geffen School of Medicine, University of California Los Angeles, Los Angeles, CA 90095, USA
[9]Department of Pathology and Laboratory Medicine, David Geffen School of Medicine, University of California Los Angeles, Los Angeles, CA 90095, USA
[10]Jonsson Comprehensive Cancer Center, David Geffen School of Medicine, University of California Los Angeles, Los Angeles, CA 90095, USA
[11]UCLA Metabolomics Center, University of California Los Angeles, Los Angeles, CA 90095, USA
[12]Crump Institute for Molecular Imaging, University of California Los Angeles, Los Angeles, CA 90095, USA
*Correspondence: jinghuang.ucla@gmail.com
http://dx.doi.org/10.1016/j.cmet.2015.06.009

SUMMARY

We discovered recently that the central metabolite α-ketoglutarate (α-KG) extends the lifespan of *C. elegans* through inhibition of ATP synthase and TOR signaling. Here we find, unexpectedly, that (*R*)-2-hydroxyglutarate ((*R*)-2HG), an oncometabolite that interferes with various α-KG-mediated processes, similarly extends worm lifespan. (*R*)-2HG accumulates in human cancers carrying neomorphic mutations in the isocitrate dehydrogenase (IDH) 1 and 2 genes. We show that, like α-KG, both (*R*)-2HG and (*S*)-2HG bind and inhibit ATP synthase and inhibit mTOR signaling. These effects are mirrored in IDH1 mutant cells, suggesting a growth-suppressive function of (*R*)-2HG. Consistently, inhibition of ATP synthase by 2-HG or α-KG in glioblastoma cells is sufficient for growth arrest and tumor cell killing under conditions of glucose limitation, e.g., when ketone bodies (instead of glucose) are supplied for energy. These findings inform therapeutic strategies and open avenues for investigating the roles of 2-HG and metabolites in biology and disease.

INTRODUCTION

Aberrant metabolism, long symbolic of inherited metabolic diseases, is now recognized as a hallmark of many other pathogenic conditions, including cancer (Warburg, 1956; Vander Heiden et al., 2009). Recently, we discovered that the common metabolite α-ketoglutarate (α-KG) increases the lifespan of adult *C. elegans* by inhibiting the highly conserved ATP synthase and the TOR pathway, mimicking dietary restriction in longevity (Chin et al., 2014). Furthermore, the observation that α-KG inhibits mTOR function in normal human cells implies a role for α-KG as an endogenous tumor suppressor metabolite (Chin et al., 2014). Known for its role in central carbon metabolism as a tricarboxylic acid (TCA) cycle intermediate, α-KG is universal to all cellular life. α-KG also serves as a co-substrate for a large family of dioxygenases with functions in cellular processes such as hypoxic response and epigenetic regulation. The identification of α-KG as a regulator of ATP synthase reveals a new mechanism for longevity regulation through metabolite signaling and suggests that there likely exist other metabolites that play signaling roles in aging. Particularly, metabolites that are similar in structure to α-KG may also modify lifespan through interactions with ATP synthase, and the lifespan effects of metabolites may correlate with their involvement in human disease.

In the TCA cycle, α-KG is produced from isocitrate by isocitrate dehydrogenase (IDH). Catalytic arginine mutations in the *IDH1* and *IDH2* genes found in gliomas and acute myeloid leukemia (AML) result in neomorphic enzymes that, instead, convert α-KG to the structurally similar (*R*)-2-hydroxyglutarate ((*R*)-2HG), which accumulates to exceedingly high levels in these patients (Dang et al., 2009; Gross et al., 2010; Ward et al., 2010; Xu et al., 2011). (*R*)-2HG is now considered an oncometabolite, impairing epigenetic and hypoxic regulation through its binding to α-KG-dependent dioxygenases (Lu

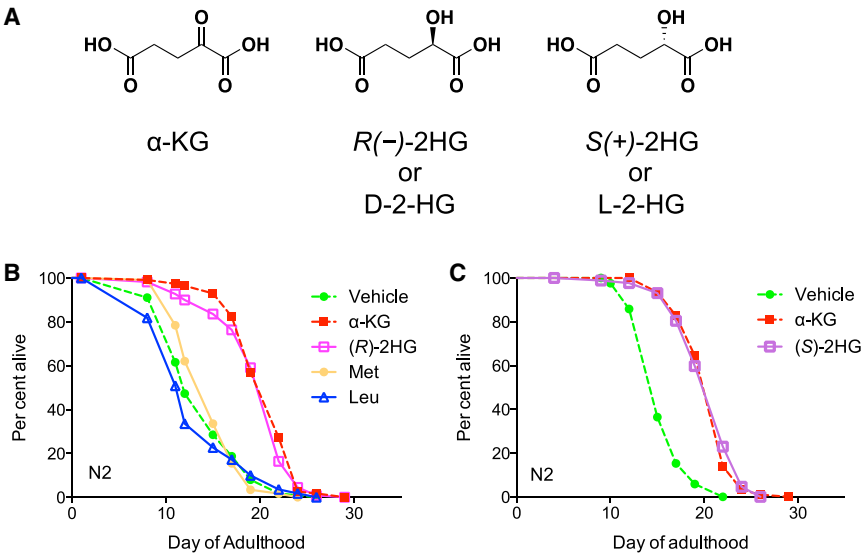

Figure 1. 2-HG Extends the Lifespan of Adult *C. elegans*

(A) Chemical structures of 2-hydroxyglutaric acid and α-ketoglutaric acid.

(B) (*R*)-2HG-supplemented worms. The mean lifespan (days of adulthood) with vehicle treatment (m_{veh}) = 14.0 (n = 112 animals tested). $m_{\alpha\text{-KG}}$ = 20.7 (n = 114), p < 0.0001 (log-rank test); $m_{(R)\text{-2HG}}$ = 20.0 (n = 110), p < 0.0001 (log-rank test); m_{Met} = 14.7 (n = 116), p = 0.4305 (log-rank test); mL_{eu} = 13.2 (n = 110), p = 0.3307 (log-rank test).

(C) (*S*)-2HG-supplemented worms. m_{veh} = 15.7 (n = 85); $m_{\alpha\text{-KG}}$ = 21.5 (n = 99), p < 0.0001 (log-rank test); $m_{(S)\text{-2HG}}$ = 20.7 (n = 87), p < 0.0001 (log-rank test).

All metabolites were given at a concentration of 8 mM. Two independent experiments were performed.

et al., 2012; Koivunen et al., 2012). The development of inhibitors of mutant IDH that normalize (*R*)-2HG levels is an attractive cancer therapeutic strategy (Wang et al., 2013; Rohle et al., 2013). Paradoxically, however, brain cancer patients with IDH mutations have a longer median overall survival than patients without mutations (Parsons et al., 2008; Yan et al., 2009; van den Bent et al., 2010), hinting at additional complexity in the biology of these cancers. (*R*)-2HG and (*S*)-2-hydroxyglutarate ((*S*)-2HG) have also been found to accumulate in tissues of individuals with germline mutations in genes encoding the corresponding 2-HG dehydrogenases (Kranendijk et al., 2012; Steenweg et al., 2010). The resulting 2-HG aciduria is associated with neurological manifestations whose molecular mechanisms are unknown (Kranendijk et al., 2010). We set out to identify additional targets of 2-HG to elucidate the mechanisms underlying the seemingly disparate 2-HG-related phenotypes.

RESULTS AND DISCUSSION

2-HG Extends the Lifespan of Adult *C. elegans*

We have demonstrated that α-KG promotes longevity through inhibition of ATP synthase (Chin et al., 2014). Given the structural similarity between α-KG and 2-HG (Figure 1A) and the association of 2-HG with cancer and neurological dysfunction, we asked whether 2-HG influences longevity. Surprisingly, both (*R*)-2HG and (*S*)-2HG increase the lifespan of *C. elegans* (Figures 1B and 1C). Notably, (*R*)-2HG, (*S*)-2HG, and α-KG interact distinctly with the α-KG-dependent dioxygenases (Koivunen et al., 2012; Tarhonskaya et al., 2014). Therefore, the similar effect of α-KG and (*R*)- and (*S*)-2-HG on lifespan points to a common mechanism that is independent of dioxygenases or any enantiomer-specific 2-HG effects (da Silva et al., 2002; Latini et al., 2005; Wajne et al., 2002; Chan et al., 2015). Because we identified the ATP synthase β subunit (ATP5B) as a target of α-KG (Chin et al., 2014), we asked whether 2-HG acts by a similar mechanism.

ATP Synthase Is a Molecular Target of 2-HG

To determine whether 2-HG targets ATP5B, we first performed a drug affinity-responsive target stability (DARTS) analysis (Lomenick et al., 2009) using U87 human glioblastoma cells. We found that both (*R*)-2HG and (*S*)-2HG bind to ATP5B (Figure 2A; data not shown). Like α-KG, both 2-HG enantiomers inhibit ATP synthase (complex V) (Figures 2B and 2C; Figures S1A–S1C). This inhibition is specific because there is no inhibition by either enantiomer on other electron transport chain (ETC) complexes (Figures S1D–S1F) or ADP import into the mitochondria (Figure S1G). The inhibition of ATP synthase by 2-HG is also readily detected in live cells. Treatment of U87 cells (wild-type IDH1/2) with membrane-permeable octyl esters of 2-HG or α-KG results in decreased cellular ATP content (Figure S2A) and a decreased ATP/ADP ratio (Figure 2D; Figure S2B) under mitochondrially oxidative phosphorylation (OXPHOS) conditions, as with the ATP synthase inhibitor oligomycin (Figures S2A and S2B). As expected, both basal and ATP synthase-linked oxygen consumption rates (OCRs) are decreased in 2-HG-treated cells (Figure 2E; Figures S2C and S2D), and lifespan increase by 2-HG is dependent on ATP synthase (Figure S2E).

IDH1(R132H) Mutant Cells Have Decreased ATP Content and Mitochondrial Respiration

At normal cellular concentrations of ~200 μM (Gross et al., 2010), (*R*)-2HG is unlikely to cause significant inhibition of ATP synthase. However, in glioma patients with IDH mutations where (*R*)-2HG accumulates to 10–100 times of natural levels (Dang et al., 2009; Gross et al., 2010), inhibition of ATP synthase would be possible. To test this idea, we used U87 cells stably expressing IDH1(R132H), the most common IDH mutation in glioma (Yan et al., 2009). Similar to octyl (*R*)-2HG-treated cells, U87/IDH1(R132H) cells exhibit decreased ATP content and ATP/ADP ratio (Figure 3A) and OCR (Figure 3B) compared with isogenic IDH1(WT)-expressing U87 cells. Importantly, the decrease in respiration in IDH1(R132H) cells is attributable to ATP synthase (complex V) inhibition. Although there is a clear difference in basal respiration rates in U87/IDH1(WT)

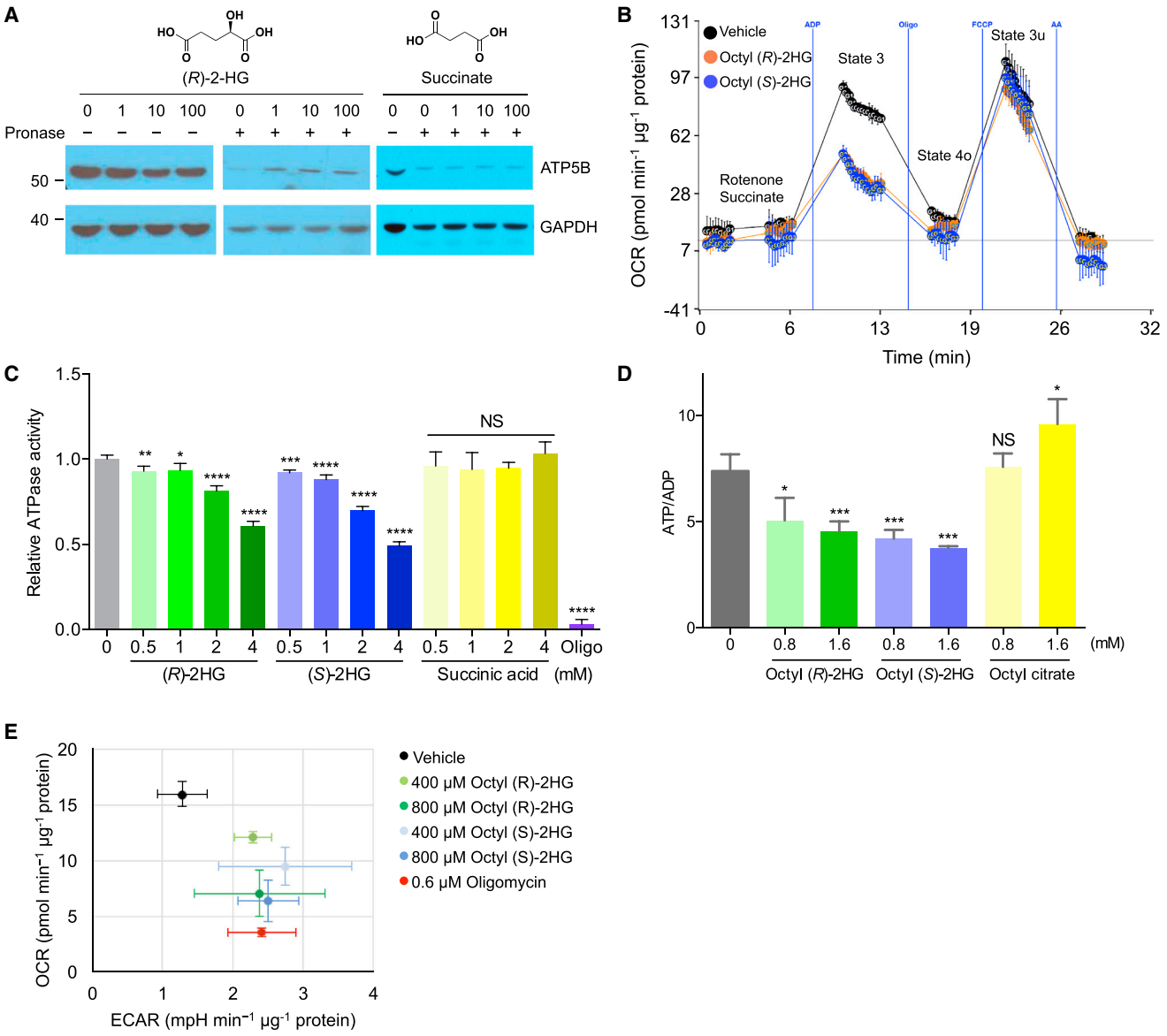

Figure 2. 2-HG Binds and Inhibits ATP Synthase

(A) DARTS identifies ATP5B as a 2-HG binding protein. U87 cell extracts were used. Succinate served as a negative control.

(B) Inhibition of ATP synthase by 2-HG. 2-HG, released from octyl 2-HG (600 µM), decreases ($p < 0.001$) state 3, but not state 4o or 3u, respiration in mitochondria isolated from mouse liver. Octanol was used as vehicle. Oligo, oligomycin; FCCP, carbonyl cyanide-*4*-(trifluoromethoxy)phenylhydrazone; AA, antimycin A.

(C) Inhibition of submitochondrial particle ATPase by 2-HG acid but not by succinic acid. *$p < 0.05$, **$p < 0.01$, ***$p < 0.001$, ****$p < 0.0001$; NS, $p > 0.05$. Oligo, oligomycin (32 µM).

(D) Decreased ATP/ADP ratio in U87 cells treated with octyl 2-HG but not octyl citrate, indicating specificity and excluding any effect involving octanol. *$p < 0.05$, ***$p < 0.001$; NS, $p > 0.05$.

(E) Decreased respiration as indicated by OCR (**$p < 0.01$) in octyl 2-HG-treated U87 cells in glucose medium. Octanol shows no effect on OCR compared with DMSO.

For (A)–(E), results were replicated in at least two independent experiments. Unpaired t test, two-tailed, two-sample unequal variance was used for (B)–(E). Mean ± SD is plotted.

versus U87/IDH1(R132H) cells, oligomycin-insensitive respiration, which is independent of complex V, is not significantly different between IDH1(WT) and IDH1(R132H) cells (Figure 3C). Furthermore, complex V knockdown using ATP5B RNAi normalizes the respiration difference between IDH1(R132H) and IDH1(WT) cells (Figure 3D). Consistently, the difference in ATP content of U87/IDH1(WT) and U87/IDH1(R132H) cells is diminished upon treatment with octyl (*R*)-2HG (Figure 3E). Similar results were obtained in HCT 116 IDH1(R132H/+) cells (Figures S3A and S3B). In addition, the mitochondrial membrane potential in IDH1 mutant cells is higher than in IDH1 wild-type cells (Figure 3F; Figure S3C), consistent with the inhibition of complex V

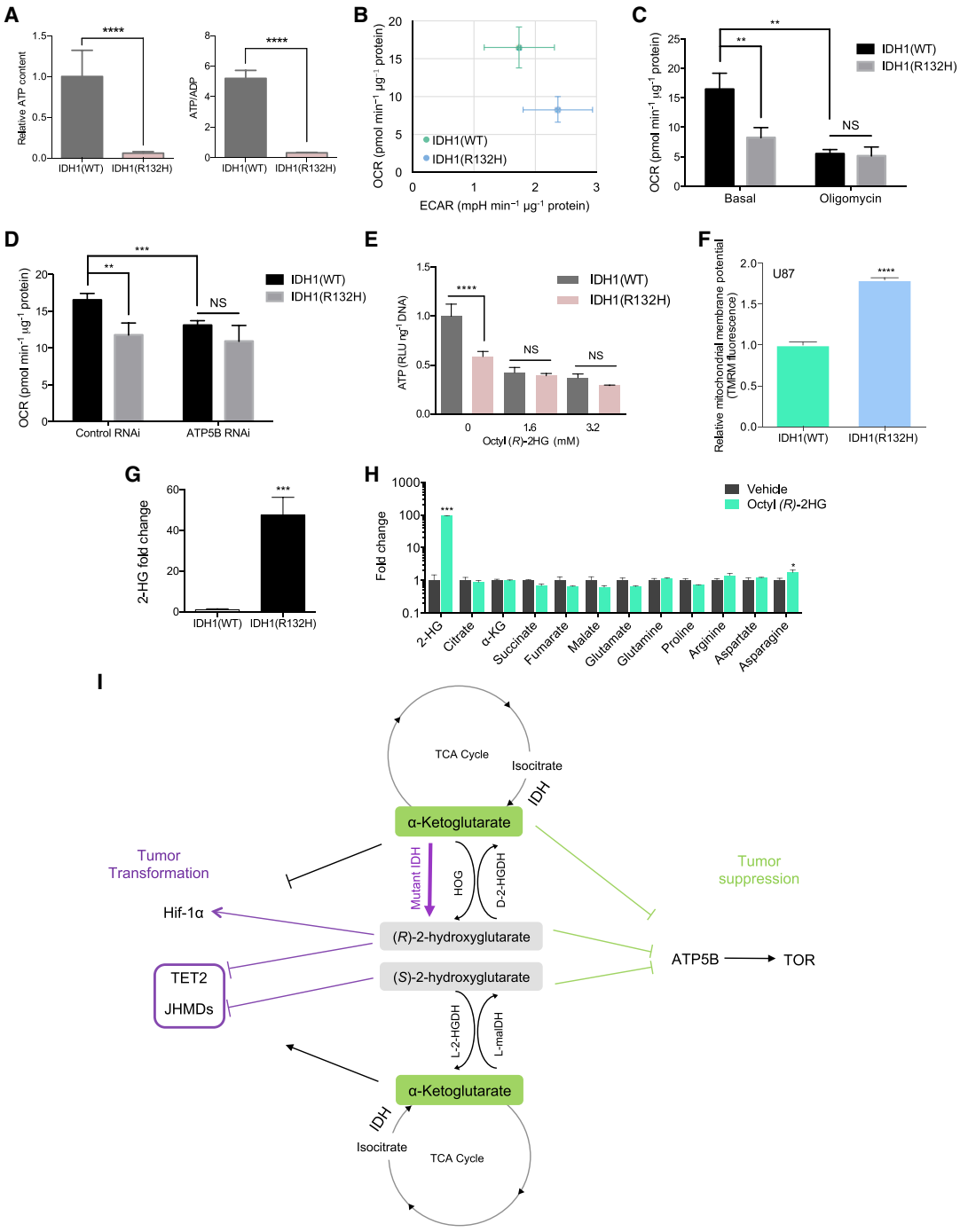

Figure 3. Inhibition of ATP Synthase in IDH1(R132H) Cells

(A) Decreased ATP levels and ATP/ADP ratio in U87/IDH1(R132H) cells (****$p < 0.0001$).

(B) Decreased respiration in U87/IDH1(R132H) cells (**$p = 0.0037$).

(C and D) Decreased respiration in U87/IDH1(R132H) cells is complex V-dependent (**$p < 0.01$, ***$p < 0.001$; NS, $p > 0.05$).

(E) Decreased ATP content in U87/IDH1(R132H) cells is attributable to (*R*)-2HG (****$p < 0.0001$; NS, $p > 0.05$).

(F) Increased mitochondrial membrane potential in U87/IDH1(R132H) cells normalized to cell number (****$p < 0.0001$).

(G) 2-HG accumulation in U87/IDH1(R132H) cells (***$p = 0.0003$).

(H) Metabolic profile of octyl *(R)*-2HG-treated U87 cells (***$p < 0.001$, *$p = 0.0435$). It is possible that the flux rate changed without affecting the absolute abundance of the intermediates.

(I) Model of metabolite signaling through ATP synthase inhibition.

Unpaired t test, two-tailed, two-sample unequal variance was used for (A)–(H). Mean ± SD is plotted. Results were replicated in at least two independent experiments.

(Johnson et al., 1981). In contrast, inhibition of ETC complex I, III, or IV causes dissipation of the mitochondrial membrane potential (Johnson et al., 1981).

The intracellular (*R*)-2HG levels are ~20- to 100-fold higher in U87 and HCT 116 cells expressing IDH1(R132H) than in control cells (Figure 3G; Figure S3D). The elevated (*R*)-2HG levels are comparable with those found in cells treated with octyl (*R*)-2HG (Figure 3H), and levels reported for IDH1 mutant tumor samples (Dang et al., 2009; Gross et al., 2010; Reitman et al., 2011). The detection of similar (*R*)-2HG levels in tumors as in octyl (*R*)-2HG-treated cells suggests that the tumor cells likely experience reduced ATP synthase and mitochondrial respiration, raising potential prognostic or therapeutic implications (see below).

2-HG Accumulation Does Not Alter the Levels of Common Metabolites

The metabolite 2-HG is linked to the TCA cycle and related amino acid metabolic pathways (Figure 3I). To explore potential metabolic changes upon octyl 2-HG treatment, we measured metabolite levels in octyl 2-HG-treated cells cultured in 1,2-^{13}C-glucose-containing medium by liquid chromatography/mass spectrometry (LC/MS). As expected, 2-HG accumulates 20- to 100-fold more after octyl 2-HG treatment (Figure 3H; Figure S3E). There is no dramatic change (<2-fold) in TCA cycle metabolites or related amino acids (Figure 3H; Figure S3E). As expected, the bulk of the increased 2-HG came from the hydrolysis of exogenously provided octyl 2-HG, as indicated by the unlabeled M+0 isotopomer (Figure S3F; data not shown for octyl (*S*)-2HG treatment). There is also no major change (<2-fold) in labeled TCA cycle intermediates and related amino acids (Figure S3G). Similarly, treatment with octyl α-KG causes an increase in α-KG levels without other substantial changes in the metabolic profile (Figure S3H). The steady-state metabolic profiles observed in 2-HG-treated (or α-KG-treated) cells support the notion that the bioenergetic shift results from the direct inhibition of ATP synthase by 2-HG (or α-KG) rather than secondary effects (Figure 3I).

IDH1(R132H) Mutant Cells Exhibit Intrinsic Vulnerability to Glucose Limitation

As the end component of the mitochondrial ETC, ATP synthase is a major source of cellular energy and the sole site for OXPHOS (Walker, 2013). When glycolysis is inhibited, for example, under conditions of glucose insufficiency, cells are forced to rely on mitochondrial respiration as a source of ATP. The inherent inhibition of ATP synthase and mitochondrial respiration in mutant IDH1 cancer cells therefore suggests a potential Achilles heel for these cancers. Supporting this idea, when cultured in glucose-free, galactose-containing medium to ensure that respiration is the primary source of energy, IDH1(R132H) cells exhibit drastically decreased cell viability (Figure 4A; Figure S4A). These results indicate a particular sensitivity of IDH1(R132H) mutant cells to the deprivation of glucose. The mutant cell line is not sensitive to fetal bovine serum (FBS) deprivation (data not shown), indicating that its increased vulnerability to glucose starvation is specific. This vulnerability to glucose starvation is also evident in U87 cells treated with octyl α-KG or octyl 2-HG (Figures 4B–4D; Figure S4B) and in ATP5B knockdown cells (Figure 4E). These findings raise the possibility that cancer cells with the IDH1(R132H) mutation (and the concomitant ATP synthase/mitochondrial respiration defect) may also be particularly sensitive to nutrient conditions analogous to glucose limitation.

In complex organisms, glucose limitation can occur as a consequence of ketosis, wherein cells use ketone bodies (instead of glucose) for energy. Ketosis is naturally induced upon prolonged starvation (or fasting), during which cells derive energy from fat reservoirs while sparing protein in muscle and other tissues from catabolism. Ketosis can also be induced by feeding a low-carbohydrate, high-fat "ketogenic diet," which has shown benefits against cancer (Stafford et al., 2010). One reason for this may be that tumor cells largely depend on glucose for growth and survival. Because the metabolism of ketone bodies depends entirely on OXPHOS, one prediction is that inhibiting ATP synthase (or other ETC components) in cancer cells would confer a survival disadvantage if ketone bodies were the only source of energy. Because U87 cells are unable to utilize ketone bodies for energy, we determined the effect of ketogenic conditions using HCT 116 cells expressing mutant IDH1. When cultured in glucose-free medium containing the ketone body *(R)*-3-hydroxybutyrate, IDH1 mutant HCT 116 cells showed a profound decrease in viability compared with the parental cells (Figure 4F), confirming the suspected metabolic weakness of IDH mutant cells. These results further support our discovery that (*R*)-2HG accumulation in mutant IDH cancer cells results in ATP synthase inhibition and also suggest novel metabolic therapeutic strategies in cancer treatment.

Decreased mTOR Signaling and Cell Growth by 2-HG

Inhibition of ATP synthase leads to decreased TOR signaling in mammalian cells, worms, and flies (Chin et al., 2014; Sun et al., 2014). We found that ATP5B knockdown (Figure 4G), treatment with octyl esters of 2-HG (Figure 4H), and IDH1(R132H) mutation (Figure 4I) all decrease the phosphorylation of mTOR complex 1 substrates. This effect occurs initially (4 h) in an AMPK-independent manner, with 2-HG decreasing mTOR signaling without significantly altering AMPK activity. However, prolonged exposure to 2-HG (24 h) also activates AMPK (Figure S4C), consistent with the idea that mTOR itself may directly sense ATP (Dennis et al., 2001) in addition to responding to AMP levels through crosstalk with AMPK (Shaw, 2009; Inoki et al., 2012).

TOR is a major regulator of cell growth (Blagosklonny and Hall, 2009). Consistent with the decreased TOR signaling, we observed growth inhibition in ATP5B knockdown cells (Figure S4D), in cells treated with octyl α-KG or octyl 2-HG (Figures S4E–S4G), and in IDH1(R132H)-expressing cells (Figures S4H and S4I). ATP5B RNAi normalizes the growth difference between IDH1(R132H) and IDH1(WT) cells (Figure S4J). Growth inhibition by 2-HG (and by α-KG) is also observed in WI-38 normal human diploid fibroblasts, in immortalized non-malignant HEK293 cells, and in other cancer cell lines tested (Figures S4K–S4N). These results suggest that, when present in excess, 2-HG acts as a growth-inhibitory metabolite across cell types. Further work is warranted to test whether the growth-inhibitory effect of (*R*)-2HG underlies the longer median overall survival of glioma patients with IDH mutations.

SUMMARY

We demonstrate that, similar to α-KG, both enantiomers of 2-HG bind and inhibit ATP synthase and extend the lifespan of

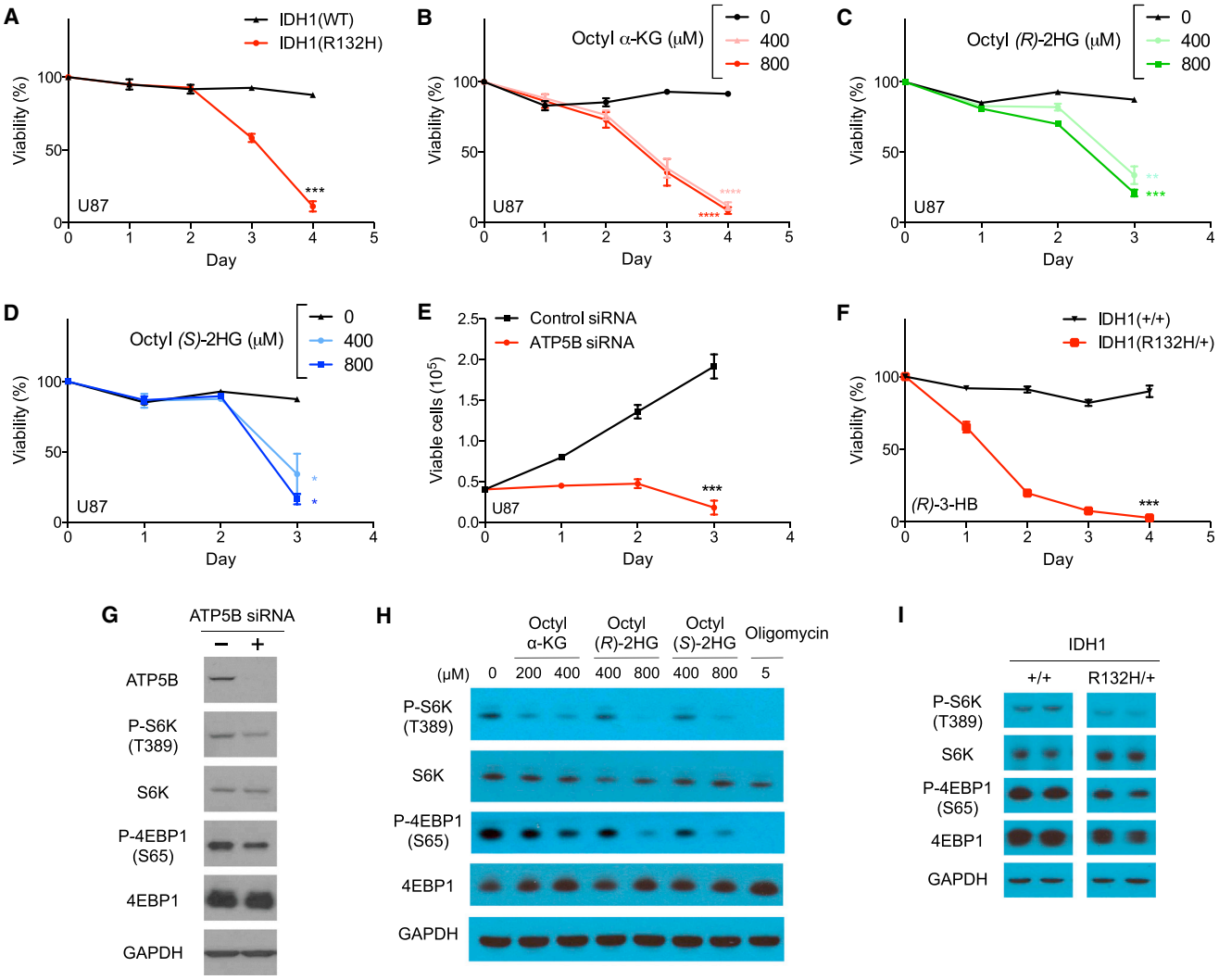

Figure 4. Inherent Vulnerability, or the Loss of Cell Viability, Characteristic of Cells with ATP5B Knockdown, 2-HG Accumulation, or IDH Mutations

(A) U87/IDH1(R132H) cells have increased vulnerability to glucose starvation (***$p < 0.001$).

(B–D) Octyl α-KG- or octyl 2-HG-treated U87 cells exhibit decreased viability upon glucose starvation (****$p < 0.0001$, ***$p < 0.001$, **$p < 0.01$, *$p < 0.05$).

(E) ATP5B knockdown inhibits U87 cell growth (***$p = 0.0004$).

(F) HCT 116 IDH1(R132H/+) cells exhibit increased vulnerability to glucose-free medium supplemented with *(R)*-3-hydroxybutyrate (***$p < 0.001$).

(G–I) U87 cells with ATP5B knockdown or octyl esters of α-KG or 2-HG treatment and HCT 116 IDH1(R132H/+) cells exhibit decreased mTOR complex 1 activity in glucose-free, galactose-containing medium.

For (A)–(E), cells were cultured in galactose medium. All lanes in (I) are on the same blot. Spaces indicate the positions of unnecessary lanes that were removed digitally. Octanol has no effect on mTOR activity. Unpaired t test, two-tailed, two-sample unequal variance was used for (A)–(F). Mean ± SD is plotted. Results in (A)–(I) were replicated in at least two independent experiments.

C. elegans. Inhibition of ATP synthase by these related metabolites decreases mitochondrial respiration and mTOR signaling. Both 2-HG and α-KG exhibit broad growth-inhibitory effects and reduce cancer cell viability under glucose-restricted conditions. It is now recognized that (*R*)-2HG, which accumulates in IDH mutant cancers, facilitates oncogenic transformation. Little is known, however, about how (*R*)-2HG modifies the phenotype of IDH mutant gliomas when the tumors are formed. Our findings suggest that, in addition to interfering with various α-KG binding factors with importance in cancer, (*R*)-2HG also acts, through inhibition of ATP synthase and mTOR signaling downstream, to decrease tumor cell growth and viability. The latter property may contribute to the improved prognosis of IDH mutant glioma patients. This idea is consistent with emerging findings that the inhibition of ETC complex I in cancer could be an effective therapeutic strategy (Wheaton et al., 2014; Birsoy et al., 2014). Together, these findings highlight a hopeful approach to cancer prevention and treatment by targeting certain aging pathways through metabolic modulation.

The effects of excess 2-HG are likely to be context-dependent. Although its growth-inhibitory effects may be beneficial in cancer, in 2-HG aciduria, the inhibition of ATP synthase and

the resulting impaired mitochondrial function could contribute to neurological dysfunction (da Silva et al., 2002; Wajne et al., 2002; Kölker et al., 2002; Latini et al., 2005). Therefore, the identification of ATP synthase as a target of both 2-HG enantiomers provides a congruent molecular basis for 2-HG-associated cancer and neurological disorders. We postulate that altered mitochondrial energy metabolism may contribute to the inverse susceptibility to cancer and neurodegenerative diseases (*e.g.*, Parkinson's disease). Finally, our findings raise the possibility that nutrient and/or metabolic intervention per se, such as diets that lower the reliance on glucose, and/or approaches that perturb cellular energy metabolism (e.g., by targeting OXPHOS), may benefit glioma patients. Such approaches may be particularly valuable for improving the survival of glioma patients without IDH mutations, who otherwise have no means to inherently curb mitochondrial respiration, and for cancer prevention and treatment in general.

EXPERIMENTAL PROCEDURES

Lifespan Analysis

Lifespan experiments were performed as described previously (Chin et al., 2014). Lifespan assays were conducted at 20°C on solid nematode growth medium (NGM). L4 or young adult animals were placed onto NGM assay plates containing D-2-HG (Sigma, catalog no. H8378), L-2-HG (Sigma, catalog no. 90790), α-KG (Sigma, catalog no. K1128), or vehicle control (H_2O). Assay plates were seeded with OP50. For RNAi experiments, NGM assay plates also contained 1 mM isopropyl-β-D-thiogalactoside (IPTG) and 50 μg/ml ampicillin and were seeded with the appropriate RNAi feeding clone (Thermo Scientific/OpenBiosystems). The *C. elegans* TOR (*let-363*) RNAi clone was obtained from Joseph Avruch (Massachusetts General Hospital/Harvard). To assess the survival of the worms, the animals were prodded with a platinum wire every 2–3 days, and those that failed to respond were scored as dead. Worms that ruptured, bagged, or crawled off the plates were censored. Lifespan data were analyzed using GraphPad Prism. *p* Values were calculated using the log-rank (Mantel-Cox) test unless stated otherwise.

Target Identification Using DARTS

DARTS was performed as described previously (Lomenick et al., 2009).

Measurement of Mitochondrial Respiration

Mitochondrial respiration was analyzed using isolated mitochondria (Brand and Nicholls, 2011). Animal studies were performed under approved University of California Los Angeles (UCLA) animal research protocols.

Cell Growth and Viability Assays

Cells were seeded in 12-well plates and, after overnight incubation, treated with the indicated concentrations of each compound. After harvesting, cells were stained with acridine orange (AO) and 4′,6-diamidino-2-phenylindole (DAPI). Cell number and viability were measured based on AO and DAPI fluorescence as measured by NC3000 (ChemoMetec) following the manufacturer's instructions.

Metabolic Profile Analysis

Cells were cultured for 24 hr and rinsed with PBS, and medium containing 1,2-^{13}C-glucose (1 g/l) was added. After 24-hr culture, cells were rinsed with ice-cold 150 mM NH_4AcO (pH 7.3), followed by addition of 400 μl cold methanol and 400 μl cold water. Cells were scraped off and transferred to an Eppendorf tube, and 10 nmol norvaline as well as 400 μl chloroform were added to each sample. For the metabolite extraction, samples were vortexed for 5 min on ice and spun down, and the aqueous layer was transferred into a glass vial and dried. Metabolites were resuspended in 70% ACN, and a 5-μl sample was loaded onto a Phenomenex Luna 3u NH2 100A (150 × 2.0 mm) column. The chromatographic separation was performed on an UltiMate 3000RSLC (Thermo Scientific) with mobile phases A (5 mM NH_4AcO [pH 9.9]) and B (ACN) and a flow rate of 300 μl/ min. The gradient ran from 15% A to 95% A over 18 min, 9 min isocratic at 95% A, and re-equilibration for 7 min. Metabolite detection was achieved with a Thermo Scientific Q Exactive mass spectrometer run in polarity switching mode (+3.0 kV / −2.25 kV). TraceFinder 3.1 (Thermo Scientific) was used to quantify metabolites as the area under the curve using retention time and accurate mass measurements (≤3 ppm). Relative amounts of metabolites were calculated by summing up all isotopomers of a given metabolite and normalized to the internal standard and cell number. Natural occurring ^{13}C was accounted for as described by Yuan et al. (2008).

Statistical Analyses

All experiments were repeated at least two times with identical or similar results. Data represent biological replicates. Appropriate statistical tests were used for every figure. Mean ± SD is plotted in all figures. See the Supplemental Experimental Procedures for details.

SUPPLEMENTAL INFORMATION

Supplemental Information includes Supplemental Experimental Procedures and four figures and can be found with this article online at http://dx.doi.org/10.1016/j.cmet.2015.06.009.

AUTHOR CONTRIBUTIONS

The majority of experiments were designed and performed by X.F.; lifespan assays by R.M.C.; DARTS by H.H.; mitochondrial respiration study design and analyses by L.V. and K.R.; enzyme inhibition assays by R.M.C.; compound syntheses by G.D., Y.X., and M.E.J.; and metabolomic profiling and analysis by X.F. and D.B. S.L., L.T., D.A.N., M.Y.P., F.F., C.C., R.M.P., M.A.T., A.L., K.F.F., M.J., S.G.C., T.F.C., T.G.G., D.B., H.R.C., M.E.J., L.V., and K.R. provided guidance, specialized reagents, and expertise. X.F., K.R., and J.H. wrote the paper. X.F., R.M.C., and J.H. analyzed data. All authors discussed the results and contributed to aspects of preparing the manuscript.

ACKNOWLEDGMENTS

We thank Chris Walsh for insightful suggestions and advice. This work was supported by the Oppenheimer Program, NIH grants R01 AT006889 and P01 HL028481, and UCLA Jonsson Cancer Center Foundation and National Center for Advancing Translational Sciences UCLA Clinical and Translational Science Institute (CTSI) Grant UL1TR000124. X.F. is a recipient of a China Scholarship Council scholarship. R.M.C. is a postdoctoral fellow supported by the UCLA Tumor Immunology Training Program (NIH T32 CA009120). M.Y.P. was a trainee of the UCLA C&MB training grant (NIH T32 GM007185). Support for L.V. and K.R. was from the Leducq Foundation. This paper is dedicated to Dr. Judith Gasson in honor of her 20 years as Director of the Jonsson Comprehensive Cancer Center.

Received: October 16, 2014
Revised: February 27, 2015
Accepted: June 10, 2015
Published: July 16, 2015

REFERENCES

Birsoy, K., Possemato, R., Lorbeer, F.K., Bayraktar, E.C., Thiru, P., Yucel, B., Wang, T., Chen, W.W., Clish, C.B., and Sabatini, D.M. (2014). Metabolic determinants of cancer cell sensitivity to glucose limitation and biguanides. Nature *508*, 108–112.

Blagosklonny, M.V., and Hall, M.N. (2009). Growth and aging: a common molecular mechanism. Aging (Albany, N.Y. Online) *1*, 357–362.

Brand, M.D., and Nicholls, D.G. (2011). Assessing mitochondrial dysfunction in cells. Biochem. J. *435*, 297–312.

Chan, S.M., Thomas, D., Corces-Zimmerman, M.R., Xavy, S., Rastogi, S., Hong, W.J., Zhao, F., Medeiros, B.C., Tyvoll, D.A., and Majeti, R. (2015). Isocitrate dehydrogenase 1 and 2 mutations induce BCL-2 dependence in acute myeloid leukemia. Nat. Med. *21*, 178–184.

Chin, R.M., Fu, X., Pai, M.Y., Vergnes, L., Hwang, H., Deng, G., Diep, S., Lomenick, B., Meli, V.S., Monsalve, G.C., et al. (2014). The metabolite α-ketoglutarate extends lifespan by inhibiting ATP synthase and TOR. Nature *510*, 397–401.

da Silva, C.G., Ribeiro, C.A., Leipnitz, G., Dutra-Filho, C.S., Wyse AT, A.T., Wannmacher, C.M., Sarkis, J.J., Jakobs, C., and Wajner, M. (2002). Inhibition of cytochrome c oxidase activity in rat cerebral cortex and human skeletal muscle by D-2-hydroxyglutaric acid in vitro. Biochim. Biophys. Acta *1586*, 81–91.

Dang, L., White, D.W., Gross, S., Bennett, B.D., Bittinger, M.A., Driggers, E.M., Fantin, V.R., Jang, H.G., Jin, S., Keenan, M.C., et al. (2009). Cancer-associated IDH1 mutations produce 2-hydroxyglutarate. Nature *462*, 739–744.

Dennis, P.B., Jaeschke, A., Saitoh, M., Fowler, B., Kozma, S.C., and Thomas, G. (2001). Mammalian TOR: a homeostatic ATP sensor. Science *294*, 1102–1105.

Gross, S., Cairns, R.A., Minden, M.D., Driggers, E.M., Bittinger, M.A., Jang, H.G., Sasaki, M., Jin, S., Schenkein, D.P., Su, S.M., et al. (2010). Cancer-associated metabolite 2-hydroxyglutarate accumulates in acute myelogenous leukemia with isocitrate dehydrogenase 1 and 2 mutations. J. Exp. Med. *207*, 339–344.

Inoki, K., Kim, J., and Guan, K.L. (2012). AMPK and mTOR in cellular energy homeostasis and drug targets. Annu. Rev. Pharmacol. Toxicol. *52*, 381–400.

Johnson, L.V., Walsh, M.L., Bockus, B.J., and Chen, L.B. (1981). Monitoring of relative mitochondrial membrane potential in living cells by fluorescence microscopy. J. Cell Biol. *88*, 526–535.

Koivunen, P., Lee, S., Duncan, C.G., Lopez, G., Lu, G., Ramkissoon, S., Losman, J.A., Joensuu, P., Bergmann, U., Gross, S., et al. (2012). Transformation by the (R)-enantiomer of 2-hydroxyglutarate linked to EGLN activation. Nature *483*, 484–488.

Kölker, S., Pawlak, V., Ahlemeyer, B., Okun, J.G., Hörster, F., Mayatepek, E., Krieglstein, J., Hoffmann, G.F., and Köhr, G. (2002). NMDA receptor activation and respiratory chain complex V inhibition contribute to neurodegeneration in d-2-hydroxyglutaric aciduria. Eur. J. Neurosci. *16*, 21–28.

Kranendijk, M., Struys, E.A., van Schaftingen, E., Gibson, K.M., Kanhai, W.A., van der Knaap, M.S., Amiel, J., Buist, N.R., Das, A.M., de Klerk, J.B., et al. (2010). IDH2 mutations in patients with D-2-hydroxyglutaric aciduria. Science *330*, 336.

Kranendijk, M., Struys, E.A., Salomons, G.S., Van der Knaap, M.S., and Jakobs, C. (2012). Progress in understanding 2-hydroxyglutaric acidurias. J. Inherit. Metab. Dis. *35*, 571–587.

Latini, A., da Silva, C.G., Ferreira, G.C., Schuck, P.F., Scussiato, K., Sarkis, J.J., Dutra Filho, C.S., Wyse, A.T., Wannmacher, C.M., and Wajner, M. (2005). Mitochondrial energy metabolism is markedly impaired by D-2-hydroxyglutaric acid in rat tissues. Mol. Genet. Metab. *86*, 188–199.

Lomenick, B., Hao, R., Jonai, N., Chin, R.M., Aghajan, M., Warburton, S., Wang, J., Wu, R.P., Gomez, F., Loo, J.A., et al. (2009). Target identification using drug affinity responsive target stability (DARTS). Proc. Natl. Acad. Sci. USA *106*, 21984–21989.

Lu, C., Ward, P.S., Kapoor, G.S., Rohle, D., Turcan, S., Abdel-Wahab, O., Edwards, C.R., Khanin, R., Figueroa, M.E., Melnick, A., et al. (2012). IDH mutation impairs histone demethylation and results in a block to cell differentiation. Nature *483*, 474–478.

Parsons, D.W., Jones, S., Zhang, X., Lin, J.C., Leary, R.J., Angenendt, P., Mankoo, P., Carter, H., Siu, I.M., Gallia, G.L., et al. (2008). An integrated genomic analysis of human glioblastoma multiforme. Science *321*, 1807–1812.

Reitman, Z.J., Jin, G., Karoly, E.D., Spasojevic, I., Yang, J., Kinzler, K.W., He, Y., Bigner, D.D., Vogelstein, B., and Yan, H. (2011). Profiling the effects of isocitrate dehydrogenase 1 and 2 mutations on the cellular metabolome. Proc. Natl. Acad. Sci. USA *108*, 3270–3275.

Rohle, D., Popovici-Muller, J., Palaskas, N., Turcan, S., Grommes, C., Campos, C., Tsoi, J., Clark, O., Oldrini, B., Komisopoulou, E., et al. (2013). An inhibitor of mutant IDH1 delays growth and promotes differentiation of glioma cells. Science *340*, 626–630.

Shaw, R.J. (2009). LKB1 and AMP-activated protein kinase control of mTOR signalling and growth. Acta Physiol. (Oxf.) *196*, 65–80.

Stafford, P., Abdelwahab, M.G., Kim, Y., Preul, M.C., Rho, J.M., and Scheck, A.C. (2010). The ketogenic diet reverses gene expression patterns and reduces reactive oxygen species levels when used as an adjuvant therapy for glioma. Nutr. Metab. (Lond) *7*, 74.

Steenweg, M.E., Jakobs, C., Errami, A., van Dooren, S.J., Adeva Bartolomé, M.T., Aerssens, P., Augoustides-Savvapoulou, P., Baric, I., Baumann, M., Bonafé, L., et al. (2010). An overview of L-2-hydroxyglutarate dehydrogenase gene (L2HGDH) variants: a genotype-phenotype study. Hum. Mutat. *31*, 380–390.

Sun, X., Wheeler, C.T., Yolitz, J., Laslo, M., Alberico, T., Sun, Y., Song, Q., and Zou, S. (2014). A mitochondrial ATP synthase subunit interacts with TOR signaling to modulate protein homeostasis and lifespan in Drosophila. Cell Rep. *8*, 1781–1792.

Tarhonskaya, H., Rydzik, A.M., Leung, I.K., Loik, N.D., Chan, M.C., Kawamura, A., McCullagh, J.S., Claridge, T.D., Flashman, E., and Schofield, C.J. (2014). Non-enzymatic chemistry enables 2-hydroxyglutarate-mediated activation of 2-oxoglutarate oxygenases. Nat. Commun. *5*, 3423.

van den Bent, M.J., Dubbink, H.J., Marie, Y., Brandes, A.A., Taphoorn, M.J., Wesseling, P., Frenay, M., Tijssen, C.C., Lacombe, D., Idbaih, A., et al. (2010). IDH1 and IDH2 mutations are prognostic but not predictive for outcome in anaplastic oligodendroglial tumors: a report of the European Organization for Research and Treatment of Cancer Brain Tumor Group. Clin. Cancer Res. *16*, 1597–1604.

Vander Heiden, M.G., Cantley, L.C., and Thompson, C.B. (2009). Understanding the Warburg effect: the metabolic requirements of cell proliferation. Science *324*, 1029–1033.

Wajne, M., Vargas, C.R., Funayama, C., Fernandez, A., Elias, M.L., Goodman, S.I., Jakobs, C., and van der Knaap, M.S. (2002). D-2-Hydroxyglutaric aciduria in a patient with a severe clinical phenotype and unusual MRI findings. J. Inherit. Metab. Dis. *25*, 28–34.

Walker, J.E. (2013). The ATP synthase: the understood, the uncertain and the unknown. Biochem. Soc. Trans. *41*, 1–16.

Wang, F., Travins, J., DeLaBarre, B., Penard-Lacronique, V., Schalm, S., Hansen, E., Straley, K., Kernytsky, A., Liu, W., Gliser, C., et al. (2013). Targeted inhibition of mutant IDH2 in leukemia cells induces cellular differentiation. Science *340*, 622–626.

Warburg, O. (1956). On the origin of cancer cells. Science *123*, 309–314.

Ward, P.S., Patel, J., Wise, D.R., Abdel-Wahab, O., Bennett, B.D., Coller, H.A., Cross, J.R., Fantin, V.R., Hedvat, C.V., Perl, A.E., et al. (2010). The common feature of leukemia-associated IDH1 and IDH2 mutations is a neomorphic enzyme activity converting alpha-ketoglutarate to 2-hydroxyglutarate. Cancer Cell *17*, 225–234.

Wheaton, W.W., Weinberg, S.E., Hamanaka, R.B., Soberanes, S., Sullivan, L.B., Anso, E., Glasauer, A., Dufour, E., Mutlu, G.M., Budigner, G.S., and Chandel, N.S. (2014). Metformin inhibits mitochondrial complex I of cancer cells to reduce tumorigenesis. eLife *3*, e02242.

Xu, W., Yang, H., Liu, Y., Yang, Y., Wang, P., Kim, S.H., Ito, S., Yang, C., Wang, P., Xiao, M.T., et al. (2011). Oncometabolite 2-hydroxyglutarate is a competitive inhibitor of α-ketoglutarate-dependent dioxygenases. Cancer Cell *19*, 17–30.

Yan, H., Parsons, D.W., Jin, G., McLendon, R., Rasheed, B.A., Yuan, W., Kos, I., Batinic-Haberle, I., Jones, S., Riggins, G.J., et al. (2009). IDH1 and IDH2 mutations in gliomas. N. Engl. J. Med. *360*, 765–773.

Yuan, J., Bennett, B.D., and Rabinowitz, J.D. (2008). Kinetic flux profiling for quantitation of cellular metabolic fluxes. Nat. Protoc. *3*, 1328–1340.

Cell Metabolism, Volume *22*

Supplemental Information

2-Hydroxyglutarate Inhibits ATP Synthase and mTOR Signaling

Xudong Fu, Randall M. Chin, Laurent Vergnes, Heejun Hwang, Gang Deng, Yanpeng Xing, Melody Y. Pai, Sichen Li, Lisa Ta, Farbod Fazlollahi, Chuo Chen, Robert M. Prins, Michael A. Teitell, David A. Nathanson, Albert Lai, Kym F. Faull, Meisheng Jiang, Steven G. Clarke, Timothy F. Cloughesy, Thomas G. Graeber, Daniel Braas, Heather R. Christofk, Michael E. Jung, Karen Reue, and Jing Huang

Supplemental Figures

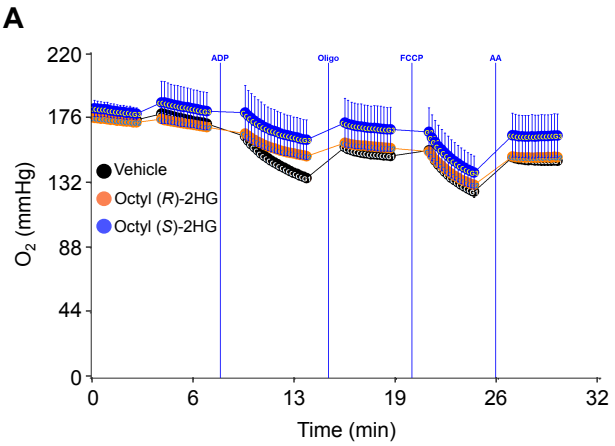

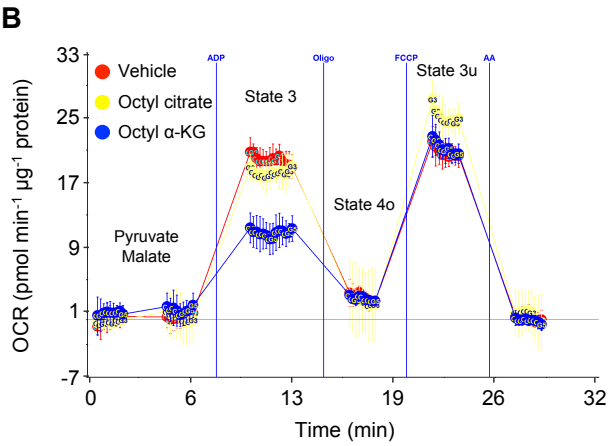

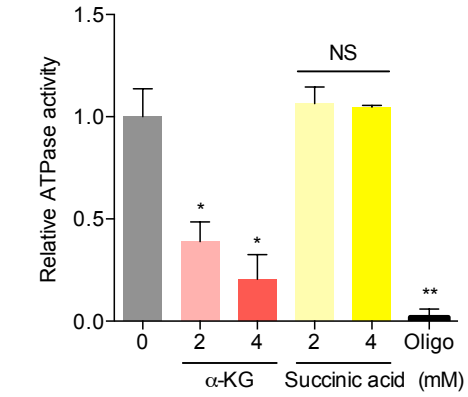

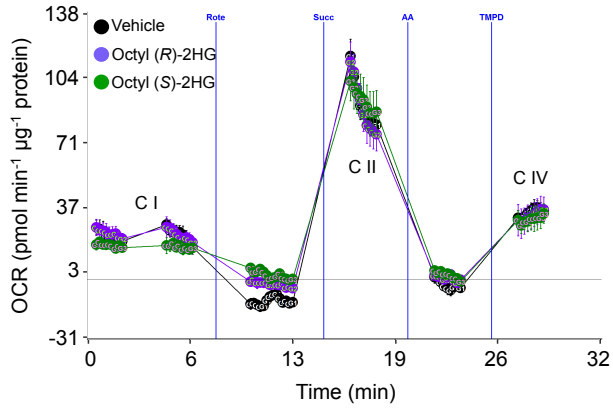

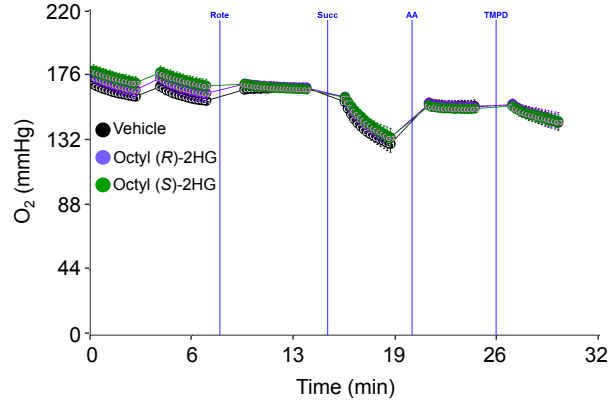

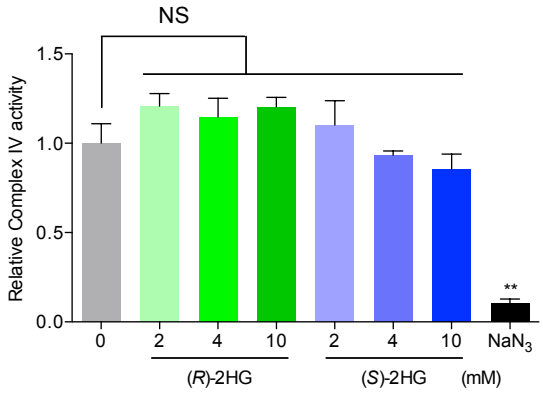

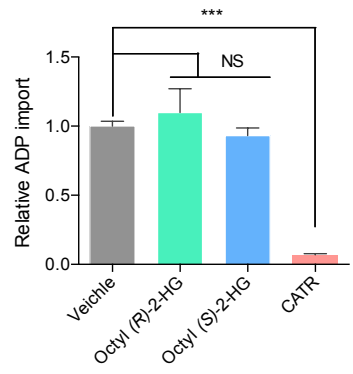

Figure S1, related to Figure 2. 2-HG does not affect the electron flow through the electron transport chain and does not affect ADP import

(A) Kinetic graphs of oxygen tension for Complex II coupling assay shown in Figure 2B, indicating that oxygen is not limiting in the assay.

(B) Octyl citrate (600 μM) has no effect on mitochondrial respiration and serves as a negative control for octyl 2-HG in Figure 2B; octyl α-KG (Chin et al., 2014) serves as a positive control.

(C) Inhibition of submitochondrial particle ATPase activity by α-KG acid and not by succinic acid (*P < 0.05, **P < 0.01; NS, P > 0.05; unpaired t-test, two-tailed, two-sample unequal variance). Oligo, oligomycin (32 μM). Mean ± s.d. is plotted.

(D) OCR from isolated mouse liver mitochondria at basal (pyruvate and malate as Complex I substrates, in presence of FCCP) and in response to sequential injection of rotenone (Rote; Complex I inhibitor), succinate (Complex II substrate), antimycin A (AA; complex III inhibitor), tetramethylphenylenediamine (TMPD; cytochrome c (Complex IV) substrate). No difference in Complex I (C I), Complex II (C II), or Complex IV (C IV) respiration is observed after 30 min treatment with 600 μM of octyl 2-HG, whereas Complex V is inhibited (Figure 2B) by the same treatment (2 independent experiments). Octanol is used as vehicle.

(E) Kinetic graphs of oxygen tension for the electron flow assay shown in (D), indicating that oxygen is not limiting in the assay.

(F) 2-HG does not inhibit Complex IV (NS, P > 0.05). NaN_3 (5 mM), a known Complex IV inhibitor, is used as positive control (**P = 0.0037; unpaired t-test, two-tailed, two-sample unequal variance). Mean ± s.d. is plotted.

(G) ADP import was measured in the presence of octanol (vehicle control) or octyl 2-HG (600 μM). Octyl *(R)*-2HG, P = 0.4237; octyl *(S)*-2HG, P = 0.1623. CATR (carboxyatractyloside, 10 μM), a known inhibitor for ADP import, was used as a positive control for the assay (***P = 0.0003). By unpaired t-test, two-tailed, two-sample unequal variance. Mean ± s.d. is plotted in all cases.

(A-G) Results were replicated in at least two independent assays.

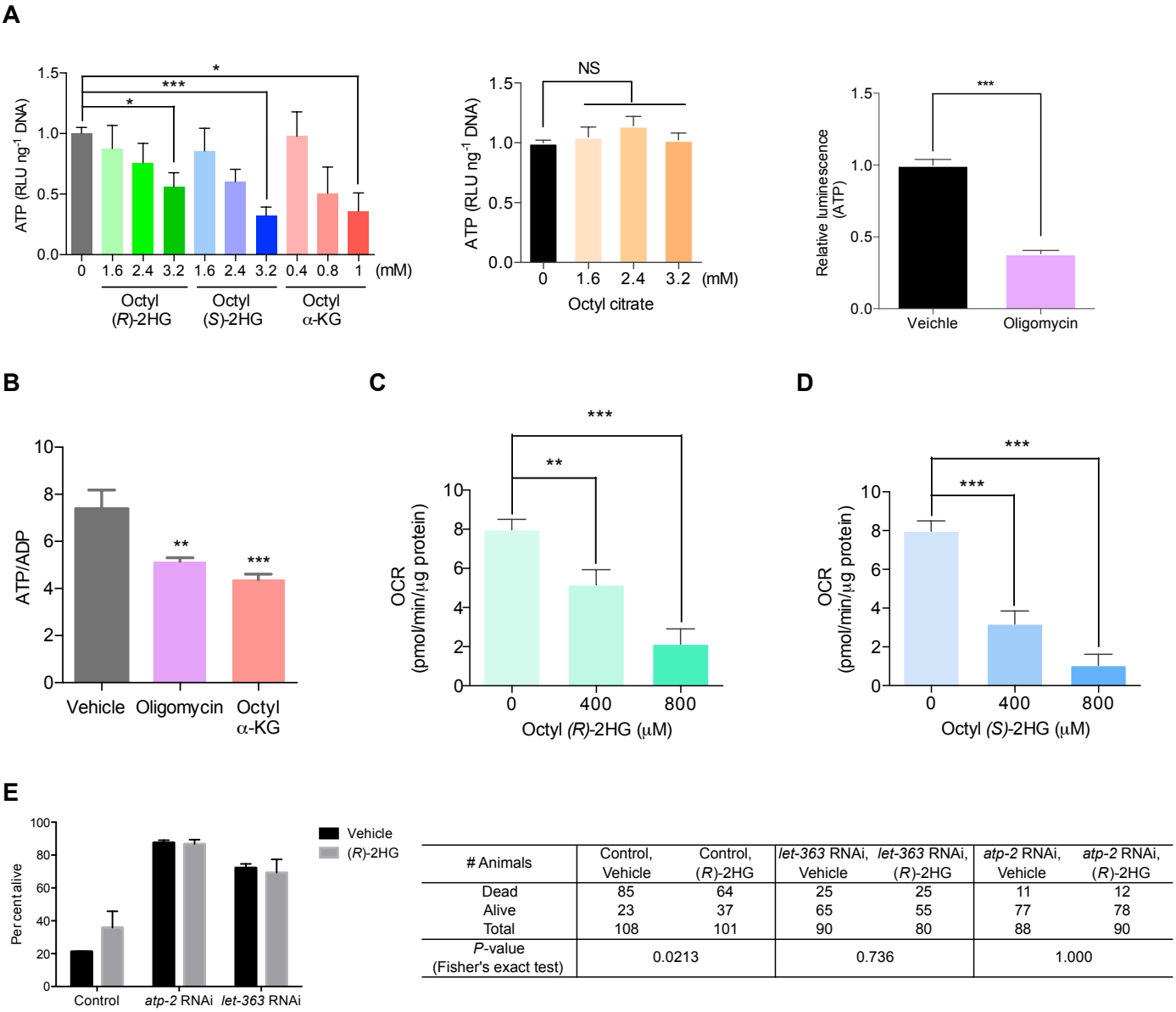

# Animals	Control, Vehicle	Control, (*R*)-2HG	*let-363* RNAi, Vehicle	*let-363* RNAi, (*R*)-2HG	*atp-2* RNAi, Vehicle	*atp-2* RNAi, (*R*)-2HG
Dead	85	64	25	25	11	12
Alive	23	37	65	55	77	78
Total	108	101	90	80	88	90
P-value (Fisher's exact test)	0.0213		0.736		1.000	

Figure S2, related to Figure 2. 2-HG inhibits cellular respiration and decreases ATP levels

(A) Decreased ATP content in U87 cells treated with octyl 2-HG or octyl α-KG (**P* < 0.05, ****P* < 0.001), but not with octyl citrate (NS, *P* > 0.05). Oligomycin (5 μM), a known inhibitor of ATP synthase, is used as a positive control. Octanol has no effect on ATP content.

(B) Octyl α-KG (800 μM) decreases ATP/ADP ratio. Oligomycin (5 μM) is a positive control. ***P* < 0.01, ****P* < 0.001.

(C-D) U87 cells treated with octyl 2-HG have decreased ATP synthase dependent (oligomycin sensitive) oxygen consumption rate (OCR) (***P* < 0.01, ****P* < 0.001).

By unpaired *t*-test, two-tailed, two-sample unequal variance.

(E) 2-HG longevity is mediated through ATP synthase and TOR. *atp-2* and *let-363* are the *C. elegans* homologs of ATP5B and TOR, respectively. Percent alive at day 19 of adulthood is plotted. **P* < 0.05, by Fisher's exact test, two-tailed.

(A-E) Results were replicated in at least two independent assays. Mean ± s.d. is plotted in all cases.

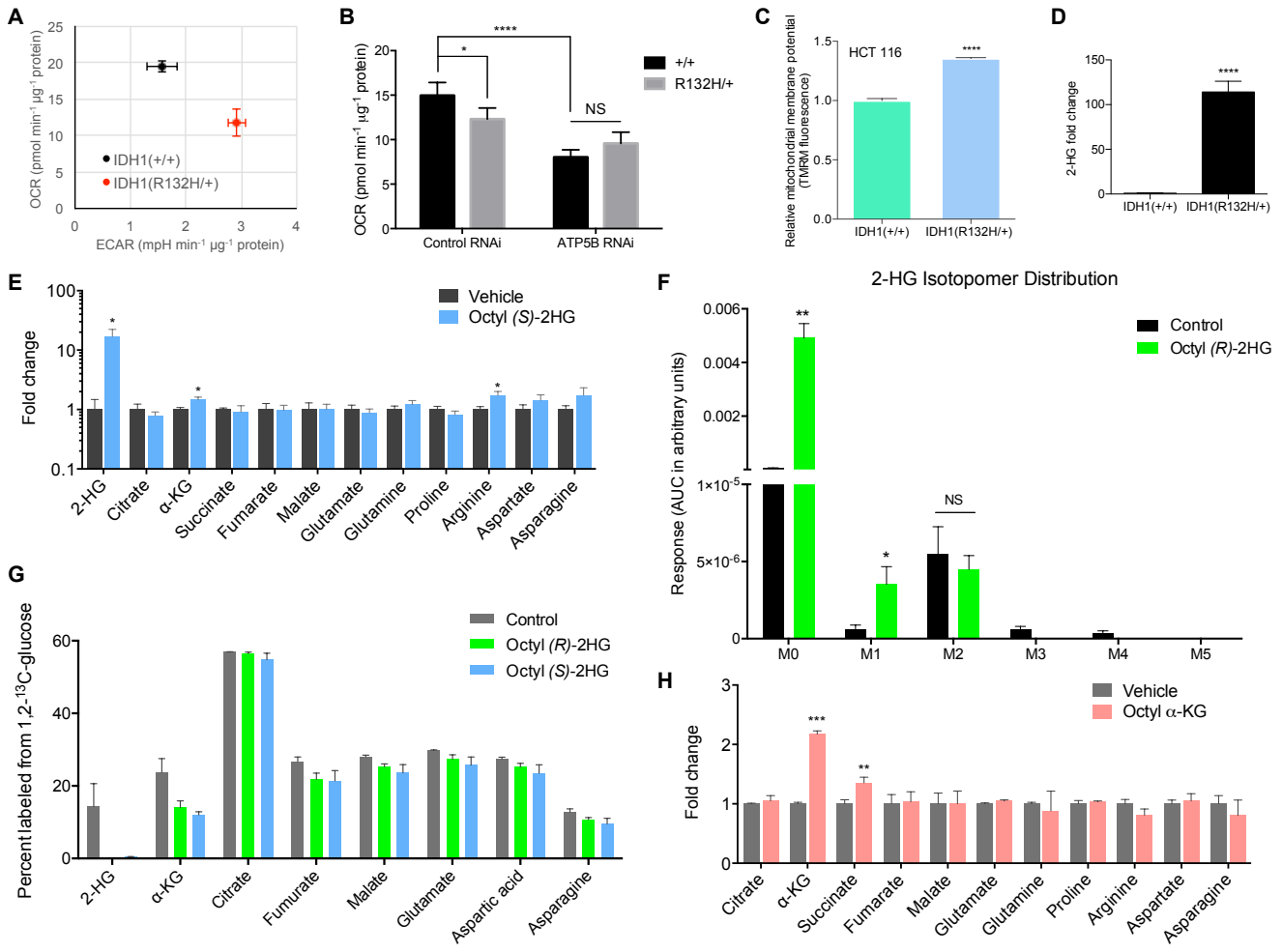

Figure S3, related to Figure 3. Cellular energetics and metabolic profiles of 2-HG accumulated cells

(A) HCT 116 IDH1(R132H/+) cells exhibit decreased respiration (***P* = 0.0015).

(B) Decreased respiration in HCT 116 IDH1(R132H/+) cells is ATP synthase dependent (**P* = 0.01; *****P* < 0.0001; NS, *P* = 0.0868).

(C) HCT 116 IDH1(R132H/+) cells exhibit increased mitochondrial membrane potential (*****P* < 0.0001); data were normalized to cell number.

(D) 2-HG levels are ~100 folder higher in HCT 116/IDH1(R132H/+) cells than in parental control cells (*****P* < 0.0001).

(E) Metabolic profile of TCA cycle intermediates and related amino acids in octyl *(S)*-2HG treated U87 cells (**P* < 0.05).

(F) 2-HG isotopomer distribution in cells cultured in medium containing 1,2-^{13}C-glucose. ***P* = 0.0039, **P* = 0.0407; NS, *P* = 0.4399.

(G) Percentage of labeled metabolites in cells cultured in medium containing 1,2-^{13}C-glucose. By unpaired *t*-test, two-tailed, two-sample unequal variance. Mean ± s.d. is plotted in all cases. Oligomycin has been reported to affect the total glucose contribution to citrate (Fendt et al., 2013). Since oligomycin inhibits the F_O subunit whereas 2-HG (and α-KG) targets the F_1 subunit, it is not likely that they will confer completely the same effects. Different levels of ATP synthase inhibition by α-KG, oligomycin, and genetic alterations are also known to elicit similar but non-identical phenotypes (Chin *et al.*, 2014).

(H) Metabolic profile of TCA cycle intermediates and related amino acids in octyl α-KG treated HEK 293 cells (***$P < 0.001$, **$P < 0.01$).
(A-G) Results were replicated in two independent experiments; (H) results were obtained from three biological replicates in one experiment.

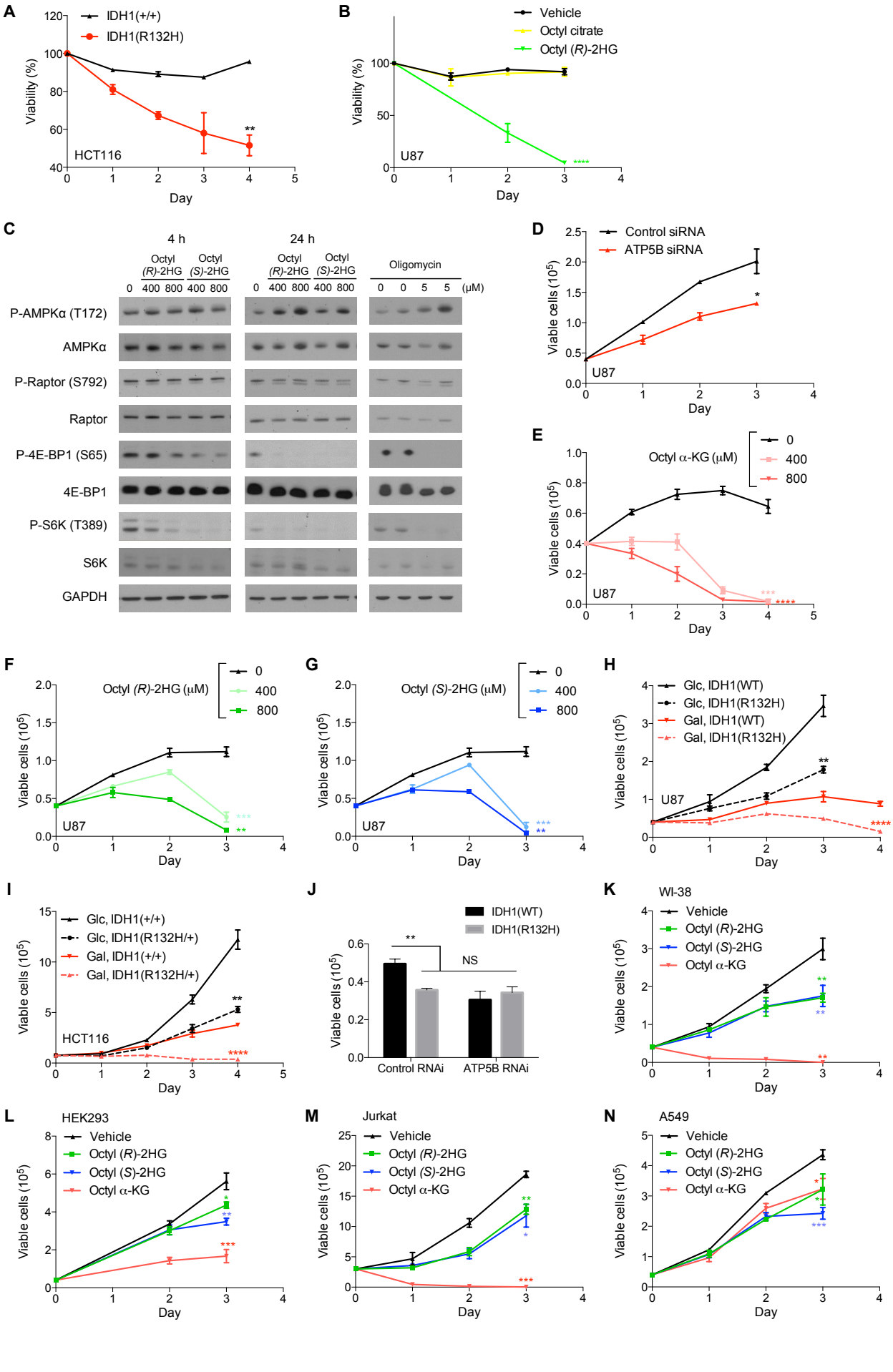
A
IDH1(+/+)
IDH1(R132H)
Viability (%)
HCT116
Day
B
Vehicle
Octyl citrate
Octyl (R)-2HG
U87
C
4 h
24 h
Octyl (R)-2HG
Octyl (S)-2HG
Oligomycin
0 400 800 400 800 0 400 800 400 800 0 0 5 5 (μM)
P-AMPKα (T172)
AMPKα
P-Raptor (S792)
Raptor
P-4E-BP1 (S65)
4E-BP1
P-S6K (T389)
S6K
GAPDH
D
Control siRNA
ATP5B siRNA
Viable cells (10^5)
U87
Day
E
Octyl α-KG (μM)
0
400
800
F
Octyl (R)-2HG (μM)
G
Octyl (S)-2HG (μM)
H
Glc, IDH1(WT)
Glc, IDH1(R132H)
Gal, IDH1(WT)
Gal, IDH1(R132H)
I
Glc, IDH1(+/+)
Glc, IDH1(R132H/+)
Gal, IDH1(+/+)
Gal, IDH1(R132H/+)
J
IDH1(WT)
IDH1(R132H)
NS
Control RNAi
ATP5B RNAi
K
WI-38
Vehicle
Octyl (R)-2HG
Octyl (S)-2HG
Octyl α-KG
L
HEK293
M
Jurkat
N
A549

Figure S4, related to Figure 4. Cells with ATP5B knockdown, octyl α-KG or octyl 2-HG treatment, or IDH mutations exhibit decreased viability and proliferation rate.
(A) HCT 116 IDH1(R132H/+) cells exhibit decreased viability upon glucose starvation. Cells were cultured in glucose-free, galactose-containing medium.
(B) Octyl citrate treated U87 cells do not exhibit altered viability upon glucose starvation. Cells were cultured in galactose medium. Octyl citrate and octyl (*R*)-2HG were each at 800 μM.
(C) mTOR complex I activity is decreased in U87 cells treated with octyl 2-HG through both an AMPK-independent and AMPK-depenent manner. Cells were cultured in glucose-free, galactose-containing medium. Phospho-raptor (S792) is not clearly modulated upon octyl 2-HG treatment, suggesting that raptor phosphorylation may not play a major role in 2-HG mediated mTOR signaling in U87 cells, consistent with results using oligomycin treatment.
(D) ATP5B knockdown decreases the growth rate of U87 cells even in glucose-containing medium.
(E-G) U87cells exhibit decreased growth rate upon treatment with octyl α-KG (E), octyl *(R)*-2HG (F), or octyl *(S)*-2HG (G) in glucose-free medium (galactose medium). In glucose-containing medium growth rate was also reduced albeit to a lesser extent (not shown).
(H) Compared to U87/IDH(WT) cells, U87/IDH1(R132H) cells exhibit decreased growth rate both in glucose-containing (Glc) and in glucose-free, galactose-contaning (Gal) media.
(I) HCT 116 IDH1(R132H/+) cells present decreased proliferation both in glucose-containing (Glc) and in glucose-free, galactose-containing (Gal) media.
(J) Reduced growth in U87/IDH1(R132H) cells is ATP synthase dependent.
(K-N) WI-38, HEK293,Jurkat, A549 cells also exhibit decreased growth rate upon treatment with octyl 2-HG or octyl α-KG in glucose-containing medium.
*****P* < 0.0001, ****P* < 0.001, ***P* < 0.01, **P* < 0.05; NS, *P* > 0.05; unpaired *t*-test, two-tailed, two-sample unequal variance. Mean ± s.d. is plotted in all cases. All growth curve results were replicated in at least two independent experimens.

Supplemental Experimental Procedures

Lifespan analysis

Lifespan experiments were performed as previously described (Chin et al., 2014). Lifespan assays were conducted at 20 °C on solid nematode growth media (NGM) using standard protocols and were replicated in at least two independent experiments. *C. elegans* were synchronized by performing either a timed egg lay (Sutphin and Kaeberlein, 2009) or an egg preparation (lysing ~100 gravid worms in 70 µl M9 buffer (Brenner, 1974), 25 µl bleach (10% sodium hypochlorite solution) and 5 µl 10 N NaOH). L4 or young adult animals were picked onto NGM assay plates containing 1.5% dimethyl sulfoxide (DMSO; Sigma, D8418), 49.5 µM 5-fluoro-2′-deoxyuridine (Sutphin and Kaeberlein, 2009)(FUDR; Sigma, F0503), and D-2-HG (Sigma, H8378), L-2-HG (Sigma, 90790), α-KG (Sigma, K1128), or vehicle control (H_2O). FUDR was included to prevent progeny production. All compounds were mixed into the NGM media after autoclaving and before solidification of the media. Assay plates were seeded with OP50. For RNAi experiments, NGM assay plates also contained 1 mM isopropyl-b-D-thiogalactoside (IPTG) and 50 µg/mL ampicillin, and were seeded with the appropriate RNAi feeding clone (Thermo Scientific / OpenBiosystems). The *C. elegans* TOR (*let-363*) RNAi clone was obtained from Joseph Avruch (MGH/Harvard). Worms were moved to new assay plates every 4 days (to ensure sufficient food was present at all times and to reduce the risk of mould contamination). To assess the survival of the worms, the animals were prodded with a platinum wire every 2–3 days, and those that failed to respond were scored as dead. Animals were assigned randomly to the experimental groups. Worms that ruptured, bagged (that is, exhibited internal progeny hatching), or crawled off the plates were censored. Lifespan data were analysed using GraphPad Prism; *P* values were calculated using the log-rank (Mantel–Cox) test unless stated otherwise.

Target identification using drug affinity responsive target stability (DARTS)

DARTS was performed as described (Lomenick et al., 2009; Lomenick et al., 2011). Briefly, U87 cells were lysed in M-PER buffer (Thermo Scientific, 78501) with the addition of protease (Roche, 11836153001) and phosphatase (50 mM NaF, 2 mM Na_3VO_4) inhibitors. Chilled TNC buffer (50 mM Tris-HCl pH 8.0, 50 mM NaCl, 10 mM $CaCl_2$) was added to the lysate, and protein concentration of the solution was measured on an aliquot by the BCA Protein Assay kit (Pierce, 23227). The remaining lysate was then incubated with vehicle control (H_2O) or varying concentrations of 2-HG or α-KG for 0.5 h at room temperature. The samples were then subjected to Pronase (Roche, 10165921001) digestions (5 min at room temperature) that were stopped by addition of SDS loading buffer and immediate heating (95 °C, 5 min). Samples were subjected to SDS-PAGE on 4-12% Bis-Tris gradient gel (Invitrogen, NP0322BOX), and Western blotting was carried out with antibodies against ATP5B (Sigma, AV48185) or GAPDH (Santa Cruz, SC25778).

Cell Culture

U87 cells were cultured in glucose-free DMEM (Life technologies, 11966-025) supplemented with 10% fetal bovine serum (FBS) and 10 mM glucose or 10 mM galactose when indicated. IDH1(R132H) and IDH1(WT) expressing U87 cells were as reported (Li et al., 2013). U87 cells are unable to utilize ketone bodies for energy (Maurer et al., 2011; Seyfried et al., 2011). HCT 116 IDH1(R132H/+) and parental control cells (Horizon Discovery, HD 104-013) were cultured in RPMI (Life technologies, 11875-093) supplemented with 10% FBS or DMEM (Life technologies, 11966-025) supplemented with 10% FBS and

10 mM glucose or 10 mM galactose. Normal human diploid fibroblasts WI-38 (ATCC, CCL-75) were cultured with EMEM (ATCC, 30-2003) supplemented with 10% FBS. HEK 293, A549, and HeLa cells were cultured with DMEM (Life technologies, 11966-065) supplemented with 10% FBS. Jurkat cells were cultured in RPMI supplemented with 10% FBS. All cells were cultured at 37°C and 5% CO2. Cells were transfected with indicated siRNA using DharmaFECT 1 Transfection Reagent by following the manufacturer's instructions. Knockdown efficiency was confirmed by Western blotting.

Assay for cellular ATP levels

For Figure S2A, U87 cells were seeded in 96-well plates at 2 x 10^4 cells per well and treated with indicated compound for 2 h in triplicate. ATP levels were measured using the CellTiter-Glo luminescent ATP assay (Promega, G7572); luminescence was read using Analyst HT (Molecular Devices). To confirm that the number of cells was consistent between treatments, cell lysates were further subjected to dsDNA staining using QuantiFluor dsDNA system (Promega). Statistical analysis was performed using GraphPad Prism (unpaired *t*-test).

Determination of ATP/ADP ratio

For Figure 2D and Figure S2B, U87 cells were seeded in 96-well plates at 10^4 cells/well and treated with indicated compound for 24 h. ATP/ADP ratios were measured by using EnzyLight ADP/ATP Ratio Assay Kit (BioAssay Systems); luminescence was read using Synergy H1m (BioTek). For Figure 3A, ATP and ADP levels were measured by LC-MS.

Measurement of oxygen consumption rates (OCR) and extracellular acidification rates (ECAR)

OCR and ECAR measurements were made using a Seahorse XF-24 analyzer (Seahorse Bioscience)(Wu et al., 2007). U87 cells were seeded in Seahorse XF-24 cell culture microplates at 50,000 cells per well in DMEM supplemented with 10% FBS and either 10 mM glucose or 10 mM galactose, and incubated O/N at 37 °C in 5% CO_2. Treatment with octyl α-KG, octyl (*R*)-2HG, octyl (*S*)-2HG, or DMSO (vehicle control) was for 1 h. Cells were washed in unbuffered DMEM (pH 7.4, 10 mM glucose) immediately prior to measurement, and maintained in this buffer with indicated concentrations of compound. OCR or ECAR were measured 3 times under basal conditions and normalized to protein concentration per well. Statistical analysis was performed using GraphPad Prism (unpaired *t*-test, two-tailed, two-sample unequal variance).

Isolation of mitochondria from mouse liver

Animal studies were performed under approved UCLA animal research protocols. Mitochondria from 3-month-old C57BL/6 mice were isolated as described (Rogers et al., 2011). Briefly, livers were extracted, minced at 4 °C in MSHE+BSA (70 mM sucrose, 210 mM mannitol, 5 mM HEPES, 1 mM EGTA, and 0.5% fatty acid free BSA, pH 7.2), and rinsed several times to remove blood. All subsequent steps were performed on ice or at 4 °C. The tissue was disrupted in 10 volumes of MSHE+BSA with a glass Dounce homogenizer (5-6 strokes) and the homogenate was centrifuged at 800 x *g* for 10 min to remove tissue debris and nuclei. The supernatant was decanted through a cell strainer and centrifuged at 8,000 x *g* for 10 min. The dark mitochondrial pellet was resuspended in MSHE+BSA and re-centrifuged at 8,000 x *g* for 10 min. The final mitochondrial pellets were used for various assays as described below.

Measurement of mitochondrial respiration

Mitochondrial respiration was analyzed using isolated mouse liver mitochondria (see (Brand and Nicholls, 2011) and refs therein). Mitochondria were isolated from mouse liver as described above. The final mitochondrial pellet was resuspended in 30 µL of MAS buffer (70 mM sucrose, 220 mM mannitol, 10 mM KH2PO4, 5 mM MgCl2, 2 mM HEPES, 1 mM EGTA, and 0.2% fatty acid free BSA, pH 7.2).
Isolated mitochondrial respiration was measured by running coupling and electron flow assays as described (Rogers et al., 2011). For the coupling assay, 5 µg of mitochondria in complete MAS buffer (MAS buffer supplemented with 10 mM succinate and 2 µM rotenone) were seeded into a XF24 Seahorse plate by centrifugation at 2,000 x *g* for 20 min at 4 °C. Just before the assay, the mitochondria were supplemented with complete MAS buffer for a total of 500 µL (with octanol or octyl 2-HG), and warmed at 37 °C for 30 min before starting the oxygen consumption rate measurements. Mitochondrial respiration begins in a coupled State 2; State 3 is initiated by 2 mM ADP; State 4o (oligomycin-insensitive, that is, complex V independent) is induced by 2.5 µM oligomycin and State 3u (FCCP-uncoupled maximal respiratory capacity) by 4 µM FCCP. Finally, 1.5 µg/mL antimycin A was injected at the end of the assay. For the electron flow assay, the MAS buffer was supplemented with 10 mM sodium pyruvate, 2 mM malate and 4 µM FCCP, and the mitochondria are seeded the same way as described for the coupling assay. After basal readings, the sequential injections were as follows: 2 µM rotenone (complex I inhibitor), 10 mM succinate (complex II substrate), 4 µM antimycin A (complex III inhibitor), and 10 mM/100 µM ascorbate/tetramethylphenylenediamine (complex IV substrate).
There is no known transporter for 2-HG in the mitochondria; transport of α-KG by the α-KG/malate shuttle is rate limiting. If unmodified 2-HG or α-KG were to be used to inhibit ATP synthase, an excessively longer incubation time – which jeopardizes mitochondrial integrity – would be required to allow intra-mitochondrial 2-HG and α-KG to accumulate. Octyl esters of 2-HG and α-KG allow rapid uptake across the intact inner mitochondrial membrane, upon which 2-HG or α-KG is produced through in situ hydrolysis by intramitochondrial esterases.

Submitochondrial particle (SMP) ATPase assay

ATP hydrolysis by ATP synthase was measured using submitochondrial particles (see (Alberts, 1994) and refs therein). Mitochondria were isolated from mouse liver as described above. The final mitochondrial pellet was resuspended in buffer A (250 mM sucrose, 10 mM Tris-HCl, 1 mM ATP, 5 mM $MgCl_2$, and 0.1 mM EGTA, pH 7.4) at 10 µg/µL, subjected to sonication on ice (Fisher Scientific Model 550 Sonic Dismembrator; medium power, alternating between 10 s intervals of sonication and resting on ice for a total of 60 s of sonication), and then centrifuged at 18,000 x *g* for 10 min at 4 °C. The supernatant was collected and centrifuged at 100,000 x *g* for 45 min at 4 °C. The final pellet (submitochondrial particles) was resuspended in buffer B (250 mM sucrose, 10 mM Tris-HCl, and 0.02 mM EGTA, pH 7.4).
Submitochondrial particles were diluted to 2.75 ng/µl in reaction buffer (40 mM Tris pH 7.5, 0.1 mg/mL BSA, 3 mM $MgCl_2$), and then incubated with either vehicle or drug for 45 min at room temperature. To start the ATPase reaction, ATP was added to a final concentration of 125 µM. The amount of phosphate produced after 6 min was determined by the Malachite Green Phosphate Assay Kit (BioAssay POMG-25H) and was used to calculate ATPase activity. Oligomycin (Cell signaling, 9996) was used as a positive control for the assay. Unmodified 2-HG and α-KG were used in the SMP assay since submitochondrial particles are essentially inside-out mitochondria that allow the otherwise inner mitochondrial membrane components access to non-membrane permeable molecules (Alberts, 1994).

Complex IV activity assay

Complex IV activity was assayed using the MitoTox OXPHOS Complex IV Activity Kit (Abcam, ab109906), according to the manufacturer's instructions.

Assay for ADP import

Freshly prepared mice liver mitochondria were suspended at 1 μg/μL in medium consisting of 220 mM mannitol, 70 mM sucrose, 2 mM HEPES, 2.74 μM antimycin A, 5 μM rotenone, 1 mM EGTA, and 10 mM potassium phosphate buffer, pH 7.4. The mitochondria suspension was incubated with designated drug for 30 min in 37 ℃. After incubation, the suspension was transferred to ice for 10 min incubation. Afterwards, 100 μM [^{3}H]ADP (specific radioactivity, 185 kBq/pmol) was added, and the mixture was immediately vortexed and incubated for 20 s on ice. The reaction was terminated by addition of 10 μM carboxyatractyloside, and the mixture was centrifuged at 10,000 g for 10 min at 4 ℃. After centrifuge, the supernatant was collected for reading and the pellet was washed twice with the same medium supplemented with 10 μM carboxyatractyloside. After washing, the pellet was lysed by the addition of 0.2 ml of 1% SDS. The radioactivity of the lysate and supernatant was determined by TRI-CARB 2300 TR liquid scintillation analyzer. The ADP-ATP translocation rate was determined by the ratio of the pellet versus the sum reading of the pellet and supernatant.

Assay for mitochondria membrane potential

Mitochondrial membrane potential was determined using the MitoPT TMRM kit (ImmunoChemistry, #9105). Readings were normalized to cell number.

Assay for mammalian TOR (mTOR) pathway activity

mTOR pathway activity in cells treated with octyl 2-HG or oligomycin was determined by the levels of phosphorylation of known mTOR substrates, including S6K (T389), 4E-BP1 (S65), AKT (S473), and ULK1 (S757) (Pullen and Thomas, 1997; Burnett et al., 1998; Brunn et al., 1997; Choo et al., 2008; Sengupta et al., 2010; Gingras et al., 2001; Sarbassov et al., 2005; Kim et al., 2011). Specific antibodies used: phospho (P)-S6K T389 (Cell Signaling, 9234), S6K (Cell Signaling, 9202S), P-4E-BP1 S65 (Cell Signaling, 9451S), 4E-BP1 (Cell Signaling, 9452S), P-AKT S473 (Cell Signaling, 4060S), AKT (Cell Signaling, 4691S), P-ULK1 S757 (Cell Signaling, 6888), ULK1 (Cell Signaling, 4773S), P-AMPKα T172 (Cell Signaling, 2535S), AMPKα (Cell Signaling, 2532S), P-Raptor S792 (Cell Signaling, 2083S), Raptor (Cell Signaling, 2280S), and GAPDH (Santa Cruz Biotechnology, 25778).

Synthesis of octyl esters of α-KG, 2-HG, and citrate

Synthesis of 1-octyl α-KG has recently been published by GD and MEJ (Jung and Deng, 2012). Syntheses of octyl (*S*)-2HG and octyl (*R*)-2HG were carried out as reported (Albert et al., 1987; Xu et al., 2011) with modifications below.

Synthesis of 1-Octyl (*S*) 2-hydroxypentanedioate (Octyl (*S*)-2HG)

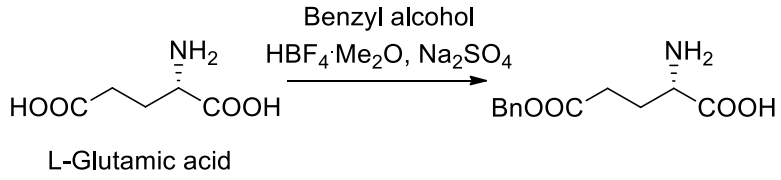

(*S*)-2-Amino-5-(benzyloxy)-5-oxopentanoic acid: L-Glutamic acid (2.0 g, 13.6 mmol) and anhydrous sodium sulfate (2.0 g) was dissolved in benzyl alcohol (25 mL), and then tetrafluoroboric acid diethyl ether

complex (3.7 mL, 27.2 mmol) was added. The suspended mixture was stirred at 21 °C overnight. Anhydrous THF (75 mL) was added to the mixture and it was filtered through a thick pad of activated charcoal. Anhydrous triethylamine (4.1 mL) was added to the clear filtrate to obtain a milky white slurry. Upon trituration with ethyl acetate (100 mL), the monoester monoacid precipitated. It was collected, washed with additional ethyl acetate (2 X 10 mL), and dried in vacuo to give the desired product (*S*)-2-amino-5-(benzyloxy)-5-oxopentanoic acid (3.07 g, 95%) as a white solid. ^{1}H NMR (500 MHz, Acetic acid-d_4): δ 7.41 – 7.25 (m, 5H), 5.14 (s, 2H), 4.12 (m, 1H), 2.75 – 2.60 (m, 2H), 2.27 (m, 2H). ^{13}C NMR (125 MHz, Acetic acid-d_4): δ 174.6, 174.4, 136.9, 129.5, 129.2, 129.1, 67.7, 55.0, 30.9, 26.3.

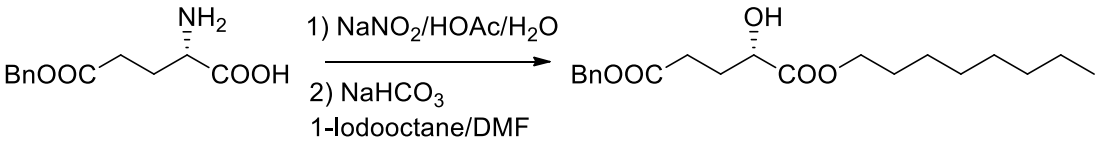

(*S*)-5-Benzyl 1-octyl 2-hydroxypentanedioate: To a solution of (*S*)-2-amino-5-(benzyloxy)-5-oxopentanoic acid (1.187 g, 5.0 mmol) in H_2O (25 mL) and acetic acid (10 mL) cooled to 0 ^{o}C was added slowly a solution of aqueous sodium nitrite (1.07 g in 15 mL H_2O). The reaction mixture was allowed to warm slowly to room temperature and was stirred overnight. The mixture was concentrated. The resulting residue was dissolved in DMF (15 mL) and $NaHCO_3$ (1.26 g, 15 mmol) and 1-iodooctane (1.84 mL, 10 mmol) were added to the mixture. The mixture was stirred at 21 °C overnight and then extracted with ethyl acetate (3 × 50 mL). The combined organic phase was washed with water and brine and dried over anhydrous $MgSO_4$. Flash column chromatography on silica gel eluting with 7/1 hexanes/ethyl acetate gave the desired mixed diester (*S*)-5-benzyl 1-octyl 2-hydroxypentanedioate (0.785 g, 45%) as a colorless oil. ^{1}H NMR (500 MHz, $CDCl_3$): δ 7.37 – 7.28 (m, 5H), 5.12 (s, 2H), 4.26 – 4.19 (m, 1H), 4.16 (t, *J* = 6.8 Hz, 2H), 3.11 (m, 1H), 2.61 – 2.46 (m, 2H), 2.26 – 2.14 (m, 1H), 1.95 (m, 1H), 1.71 – 1.57 (m, 2H), 1.39 – 1.20 (m, 10H), 0.88 (t, *J* = 6.9 Hz, 3H). ^{13}C NMR (125 MHz, $CDCl_3$): δ 174.6, 172.8, 135.8, 128.4, 128.1, 128.0, 69.3, 66.2, 65.8, 31.6, 29.6, 29.2, 29.0 (2C's), 28.4, 25.6, 22.5, 13.9.

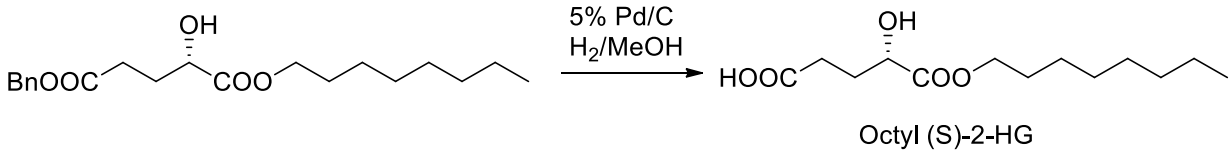

Octyl (S)-2-HG

1-Octyl (*S*) 2-hydroxypentanedioate (octyl (*S*)-2-hydroxyglutarate; octyl (*S*)-2HG): To a solution of (*S*)-5-benzyl 1-octyl 2-hydroxypentanedioate (0.71 g, 2.0 mmol) in MeOH (50 mL) was added 5% Pd/C (80 mg). Over the mixture was passed argon and then the argon was replaced with hydrogen and the mixture was stirred vigorously for 1 h. The mixture was filtered through a thick pad of Celite and the organic phase was evaporated. The residue was purified via flash column chromatography on silica gel eluting with 25/1 CH_2Cl_2/MeOH to give octyl (*S*)-2HG (0.495 g, 48%) as a white solid. ^{1}H NMR (500 MHz, $CDCl_3$): δ 4.23 (dd, *J* = 8.0, 4.2 Hz, 1H), 4.16 (t, *J* = 6.8 Hz, 2H), 2.60 – 2.42 (m, 2H), 2.15 (m, 1H), 1.92 (m, 1H), 1.69 – 1.59 (m, 2H), 1.38 – 1.16 (m, 10H), 0.86 (t, *J* = 7.0 Hz, 3H). ^{13}C NMR (125 MHz, $CDCl_3$): δ 178.8, 174.8, 69.3, 66.1, 31.7, 29.4, 29.1 (2C's), 28.9, 28.4, 25.7, 22.5, 14.0.

Synthesis of 1-Octyl (*R*) 2-hydroxypentanedioate (Octyl (*R*)-2HG)

The synthesis of the opposite enantiomer, i.e., Octyl (*R*)-2HG, was carried out by the exact same procedure starting with D-glutamic acid. The spectroscopic data was identical to that of the enantiomeric compounds.

Synthesis of 1-octyl citrate ester (Kotick, 1991; Weaver and Gilbert, 1997; Takeuchi et al., 1999)

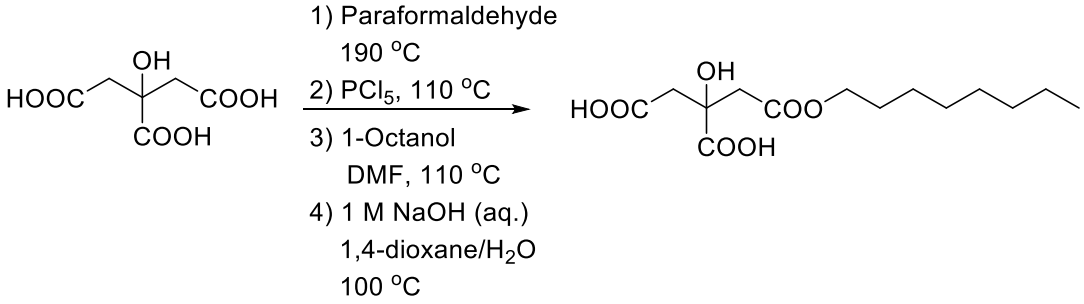

The mixture of citric acid (3.862 g, 0.02 mol) and paraformaldehyde (1.276 g, 0.04 mol) was stirred at 190 °C for 2 h. After cooling down to room temperature, the mixture was purified by flash column chromatography on silica gel eluting with 10/1 dichloromethane/methanol gave the desired methylene acetal of citric acid. The diacetic acid product (0.816 g, 4.0 mmol) and phosphorus (V) chloride (0.850 g, 4.0 mmol) were stirred with heating from room temperature to 110 °C in 1 h and kept at 110 °C until there was no further emission of hydrogen chloride. After cooling the mixture to room temperature, the phosphorus oxychloride was evaporated under vacuum. The residue was dissolved in ethyl acetate, the mixture was filtered, and the organic phase was evaporated. The resulting residue was dissolved in DMF (3.0 mL) and 1-octanol (1.89 mL, 0.012 mol) was added. The mixture was heated to 110 °C for 3 h and then extracted with ethyl acetate (3 × 50 mL). The combined organic phase was washed with water and brine and dried over anhydrous $MgSO_4$. Flash column chromatography on silica gel eluting with 15/1 dichloromethane/methanol gave the mono-octyl methylene acetal of citric acid ester (0.652 g, 52%) as a colorless oil. This mono-octyl ester (0.2576 g, 0.814 mmol) was dissolved in 1,4-dioxane (3.0 mL) and H_2O (3.0 mL). An aqueous solution of NaOH (1.0 M, 0.82 mL) was added to the mixture and the temperature was raised to 100 °C for 2 h. After cooling down the mixture to room temperature, an aqueous solution of NaOH (0.2 M, 10 mL) was added. The mixture was extracted with ethyl acetate (3 X 10mL) and the aqueous phase was acidified with 1.0 M aqueous HCl to pH 1. The acidified aqueous layer was extracted with ethyl acetate (3 X 30 mL), and the combined organic phases were washed with water and brine and dried over anhydrous $MgSO_4$. Flash column chromatography on silica gel, eluting with 10/1 dichloromethane/methanol, gave the 1-octyl citrate ester as an oil (0.183 g, 74%). ^{1}H NMR (500 MHz, $CDCl_3$) δ 10.55 (s, 2H), 4.05 (t, J = 6.5 Hz, 2H), 2.88 (m, 4H), 1.57 (m, 2H), 1.23 (m, 10H), 0.84 (t, J = 6.2 Hz, 3H). ^{13}C NMR (125 MHz, $CDCl_3$) δ 177.63, 174.68, 170.08, 72.82, 65.45, 42.81, 42.69, 31.63, 29.03, 29.01, 28.25, 25.66, 22.48, 13.92.

Supplemental References

Albert, R., Danklmaier, J., Honig, H., and Kandolf, H. (1987). A Simple and Convenient Synthesis of Beta-Aspartates and Gamma-Glutamates. Synthesis-Stuttgart, 635-637.

Alberts, B. (1994). Molecular biology of the cell. (New York: Garland Pub.).

Brand, M.D., and Nicholls, D.G. (2011). Assessing mitochondrial dysfunction in cells. Biochem J *435*, 297-312.

Brenner, S. (1974). The genetics of Caenorhabditis elegans. Genetics *77*, 71-94.

Brunn, G.J., Hudson, C.C., Sekulic, A., Williams, J.M., Hosoi, H., Houghton, P.J., Lawrence, J.C., Jr., and Abraham, R.T. (1997). Phosphorylation of the translational repressor PHAS-I by the mammalian target of rapamycin. Science *277*, 99-101.

Burnett, P.E., Barrow, R.K., Cohen, N.A., Snyder, S.H., and Sabatini, D.M. (1998). RAFT1 phosphorylation of the translational regulators p70 S6 kinase and 4E-BP1. Proc Natl Acad Sci U S A *95*, 1432-1437.

Choo, A.Y., Yoon, S.O., Kim, S.G., Roux, P.P., and Blenis, J. (2008). Rapamycin differentially inhibits S6Ks and 4E-BP1 to mediate cell-type-specific repression of mRNA translation. Proc Natl Acad Sci U S A *105*, 17414-17419.

Fendt, S.M., Bell, E.L., Keibler, M.A., Olenchock, B.A., Mayers, J.R., Wasylenko, T.M., Vokes, N.I., Guarente, L., Vander Heiden, M.G., and Stephanopoulos, G. (2013). Reductive glutamine metabolism is a function of the alpha-ketoglutarate to citrate ratio in cells. Nat Commun *4*, 2236.

Gingras, A.C., Raught, B., Gygi, S.P., Niedzwiecka, A., Miron, M., Burley, S.K., Polakiewicz, R.D., Wyslouch-Cieszynska, A., Aebersold, R., and Sonenberg, N. (2001). Hierarchical phosphorylation of the translation inhibitor 4E-BP1. Genes Dev *15*, 2852-2864.

Jung, M.E., and Deng, G. (2012). Synthesis of the 1-monoester of 2-ketoalkanedioic acids, for example, octyl alpha-ketoglutarate. J Org Chem *77*, 11002-11005.

Kim, J., Kundu, M., Viollet, B., and Guan, K.L. (2011). AMPK and mTOR regulate autophagy through direct phosphorylation of Ulk1. Nat Cell Biol *13*, 132-141.

Kotick, M.P. (1991). Method for regioselective preparation of 1- or 2-monoalkyl citrates as surfactants. U.S. Patent *US5049699*, A19910917.

Li, S., Chou, A.P., Chen, W., Chen, R., Deng, Y., Phillips, H.S., Selfridge, J., Zurayk, M., Lou, J.J., Everson, R.G., et al. (2013). Overexpression of isocitrate dehydrogenase mutant proteins renders glioma cells more sensitive to radiation. Neuro Oncol *15*, 57-68.

Lomenick, B., Jung, G., Wohlschlegel, J.A., and Huang, J. (2011). Target identification using drug affinity responsive target stability (DARTS). Curr Protoc Chem Biol *3*, 163-180.

Maurer, G.D., Brucker, D.P., Bahr, O., Harter, P.N., Hattingen, E., Walenta, S., Mueller-Klieser, W., Steinbach, J.P., and Rieger, J. (2011). Differential utilization of ketone bodies by neurons and glioma cell lines: a rationale for ketogenic diet as experimental glioma therapy. BMC Cancer *11*, 315.

Pullen, N., and Thomas, G. (1997). The modular phosphorylation and activation of p70s6k. FEBS Lett *410*, 78-82.

Rogers, G.W., Brand, M.D., Petrosyan, S., Ashok, D., Elorza, A.A., Ferrick, D.A., and Murphy, A.N. (2011). High throughput microplate respiratory measurements using minimal quantities of isolated mitochondria. PLoS One *6*, e21746.

Sarbassov, D.D., Guertin, D.A., Ali, S.M., and Sabatini, D.M. (2005). Phosphorylation and regulation of Akt/PKB by the rictor-mTOR complex. Science *307*, 1098-1101.

Sengupta, S., Peterson, T.R., and Sabatini, D.M. (2010). Regulation of the mTOR complex 1 pathway by nutrients, growth factors, and stress. Mol Cell *40*, 310-322.

Seyfried, T.N., Kiebish, M.A., Marsh, J., Shelton, L.M., Huysentruyt, L.C., and Mukherjee, P. (2011). Metabolic management of brain cancer. Biochim Biophys Acta *1807*, 577-594.

Sutphin, G.L., and Kaeberlein, M. (2009). Measuring Caenorhabditis elegans life span on solid media. J Vis Exp.

Takeuchi, Y., Nagao, Y., Toma, K., Yoshikawa, Y., Akiyama, T., Nishioka, H., Abe, H., Harayama, T., and Yamamoto, S. (1999). Synthesis and siderophore activity of vibrioferrin and one of its diastereomeric isomers. Chemical & Pharmaceutical Bulletin *47*, 1284-1287.

Weaver, R., and Gilbert, I.H. (1997). The design and synthesis of nucleoside triphosphate isosteres as potential inhibitors of HIV reverse transcriptase. Tetrahedron *53*, 5537-5562.

Wu, M., Neilson, A., Swift, A.L., Moran, R., Tamagnine, J., Parslow, D., Armistead, S., Lemire, K., Orrell, J., Teich, J., et al. (2007). Multiparameter metabolic analysis reveals a close link between attenuated mitochondrial bioenergetic function and enhanced glycolysis dependency in human tumor cells. Am J Physiol Cell Physiol *292*, C125-136.